Water and heat: new constraints on the evolution of the CV chondrite parent body

Lydie Bonal, J. Gattacceca, Alexandre Garenne, Jolantha Eschrig, Pierre Rochette, Lisa Krämer Ruggiu

▶ **To cite this version:**

Lydie Bonal, J. Gattacceca, Alexandre Garenne, Jolantha Eschrig, Pierre Rochette, et al.. Water and heat: new constraints on the evolution of the CV chondrite parent body. Geochimica et Cosmochimica Acta, 2020, 10.1016/j.gca.2020.03.009 . hal-02514824

HAL Id: hal-02514824
https://hal.science/hal-02514824v1

Submitted on 13 Jun 2020

HAL is a multi-disciplinary open access archive for the deposit and dissemination of scientific research documents, whether they are published or not. The documents may come from teaching and research institutions in France or abroad, or from public or private research centers.

L'archive ouverte pluridisciplinaire **HAL**, est destinée au dépôt et à la diffusion de documents scientifiques de niveau recherche, publiés ou non, émanant des établissements d'enseignement et de recherche français ou étrangers, des laboratoires publics ou privés.

Distributed under a Creative Commons Attribution - NonCommercial - NoDerivatives 4.0 International License

Journal Pre-proofs

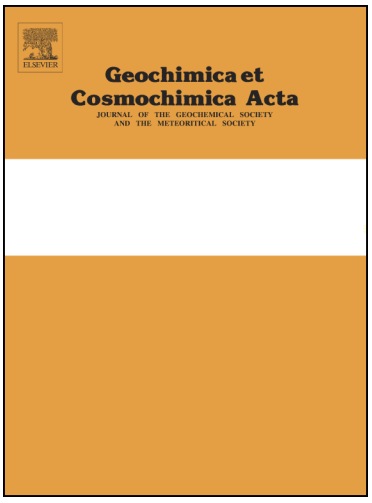

WATER AND HEAT: NEW CONSTRAINTS ON THE EVOLUTION OF THE CV CHONDRITE PARENT BODY

Lydie Bonal, Jérôme Gattacceca, Alexandre Garenne, Jolantha Eschrig, Pierre Rochette, Lisa Krämer Ruggiu

PII: S0016-7037(20)30170-8
DOI: https://doi.org/10.1016/j.gca.2020.03.009
Reference: GCA 11686

To appear in: *Geochimica et Cosmochimica Acta*

Received Date: 25 June 2019
Accepted Date: 7 March 2020

Please cite this article as: Bonal, L., Gattacceca, J., Garenne, A., Eschrig, J., Rochette, P., Krämer Ruggiu, L., WATER AND HEAT: NEW CONSTRAINTS ON THE EVOLUTION OF THE CV CHONDRITE PARENT BODY, *Geochimica et Cosmochimica Acta* (2020), doi: https://doi.org/10.1016/j.gca.2020.03.009

This is a PDF file of an article that has undergone enhancements after acceptance, such as the addition of a cover page and metadata, and formatting for readability, but it is not yet the definitive version of record. This version will undergo additional copyediting, typesetting and review before it is published in its final form, but we are providing this version to give early visibility of the article. Please note that, during the production process, errors may be discovered which could affect the content, and all legal disclaimers that apply to the journal pertain.

© 2020 Elsevier Ltd. All rights reserved.

Journal Pre-proofs

WATER AND HEAT: NEW CONSTRAINTS ON THE EVOLUTION OF THE CV CHONDRITE PARENT BODY

Lydie Bonal[1], Jérôme Gattacceca[2], Alexandre Garenne[1,3], Jolantha Eschrig[1], Pierre Rochette[2], Lisa Krämer Ruggiu[2]

[1]Institut de Planétologie et d'Astrophysique de Grenoble, Université Grenoble Alpes, CNRS CNES, 38000 Grenoble (France)

[2] CNRS, Aix Marseille Univ, IRD, Coll France, INRAE, CEREGE, Aix-en-Provence, France

[3]Nuclear and Chemical Sciences Division, Lawrence Livermore National Laboratory, Livermore, CA, USA

Corresponding author: lydie.bonal@univ-grenoble-alpes.fr

Journal Pre-proofs

ABSTRACT

This paper focuses on the post-accretion history of CV3 chondrites, through a combination of petrographic and mineralogical characterization, magnetic measurements, spectral (Raman and Infrared) and thermo-gravimetric analysis of 31 meteorites (including 7 falls, 21 Antarctic and 3 non-Antarctic finds) spanning a wide metamorphic range.

We classify the 21 Antarctic chondrites and the Bukhara fall into the CV_{Red}, CV_{OxA}, and CV_{OxB} subgroups. We establish quantitative parameters relevant for this sub-classification. In comparison to CV_{Ox}, CV_{Red} chondrites are characterized by *(i)* a lower abundance of matrix, *(ii)* a higher abundance of metal, *(iii)* the presence of Ni-poor sulfides. In comparison to CV_{OxB}, CV_{OxA} are characterized by *(i)* similar matrix abundance, *(ii)* a higher abundance of

metal, *(iii)* the presence of metal almost exclusively under the form of awaruite, (iv) lower Ni content of sulfides, (v) lower magnetic susceptibility and saturation remanence.

Both CV_{Ox} (CV_{OxA} and CV_{OxB}) and CV_{Red} experienced aqueous alteration, and contain oxyhydroxides and phyllosilicates. We show that the abundance of these hydrated secondary minerals observed today in individual CV chondrites decreases with their peak metamorphic temperature. This is interpreted either as partial dehydration of these secondary minerals or limited hydration due to the rapid exhaustion of the water reservoir during parent body thermal metamorphism. Moreover, the lower abundance of oxyhydroxides (that have a lower thermal stability than phyllosilicates and may in large part postdate the peak of thermal metamorphism) in more metamorphosed CV chondrites is interpreted as lower availability of aqueous fluids during retrograde metamorphism in these meteorites.

Lastly, we show that in comparison to CV_{OxB}, CV_{OxA} are systematically *(i)* more metamorphosed, *(ii)* less hydrated, *(iii)* depleted in ferromagnetic minerals, *(iv)* but enriched in metal in the form of secondary awaruite. CV_{OxA} may be thermally metamorphosed CV_{OxB}. CV_{Red} are significantly different from CV_{Ox} (matrix abundances, alteration products, opaque minerals), but span the same wide metamorphic range. This could be indicative of a laterally heterogeneous CV parent body, or suggest the existence of distinct parent bodies for CV_{Ox} and CV_{Red} chondrites.

Journal Pre-proofs

1. INTRODUCTION

The CV carbonaceous chondrites reveal a vast amount of information about the processes operating in the early Solar System. Indeed, they have experienced a variety of post-accretion processes, including aqueous alteration, thermal metamorphism and metasomatism. CV chondrites are characterized by the presence of the largest refractory inclusions (CAIs) of all meteorites. Measurements of long-lived and short-lived radionuclides and their interpretation in terms of absolute and relative dating (e.g., Lee et al., 1977; Amelin et al., 2010), make CV chondrites particularly popular in the cosmochemistry community as the age of CAIs is considered as the age of Solar System formation (e.g., McKeegan and Davis, 2005). Various chronometers can be applied to chondrites and to specific mineral phases to date distinct events. In particular, in addition to chondrules ages, timescales of aqueous alteration can constrain the time of accretion of chondrite parent body. It has been thereby inferred through ^{53}Mn-^{53}Cr dating of fayalite combined with thermal modeling that the CV3 parent body accreted ~ 1.8 - 2.5 Myr (Doyle et al., 2015) or ~ 3.2 - 3.3 Myr (Jogo et al. 2017) after CAIs formation. Considering several constraints such as the ages, the temperatures during fayalite formation and rough estimation of metamorphic temperatures, Jogo et al. (2017) determined that the CV3 parent body was at least 110 - 150 km in radius. This size range is consistent with modeling studies calling for a radius > ~ 200 km to account for the paleomagnetic record of a core dynamo. This record also implies a protracted style of accretion (e.g., Elkins-Tanton et al., 2011).

Identifying each of the post-accretion processes and disentangling their respective consequences is not an easy task. The understanding of the mineralogical, petrographic, and chemical modifications is challenging and subject to debates and controversies in the literature. In a pioneering paper, McSween (1977) emphasized that CV chondrites are particularly petrographically complex and diverse. Mostly based on the modal abundances of

magnetite and Fe,Ni metal in matrix and chondrules, CV chondrites were divided into oxidized (CV_{Ox}) and reduced (CV_{Red}) subgroups (McSween, 1977). The oxidized subgroup was later further subdivided into Allende-like (CV_{OxA}) and Bali-like (CV_{OxB}), based on a combination of chemical and petrographic criteria (abstract by Weisberg et al., 1997; see also review by Krot et al., 1998). These sub-classifications, although based on a limited number of samples, highlight the mineralogical diversity of the CV chondrite group.

CV_{OxB} chondrites (Bali, Kaba, Mokoia, Grosnaja for the falls) have experienced parent body aqueous alteration to variable extents, as unambiguously evidenced by the presence of phyllosilicates. Based on transmission electron microscopy, Fe-bearing saponite is observed in the matrix of Kaba (Keller and Buseck, 1990) and Mokoia (Tomeoka and Buseck, 1990), and Mg-rich saponite in the matrix of Bali (Keller et al., 1994). Different types of phyllosilicates are observed in the matrix of Grosnaja, mostly serpentine containing significant Fe (Keller and McKay, 1993). Phyllosilicates are observed not only in inter-chondrule matrix, but also within CAIs and chondrules (e.g., Cohen et al., 1983; Keller and Buseck, 1990; Keller et al., 1994; Kimura and Ikeda, 1998; Tomeoka and Buseck, 1990). Howard et al. (2010) measured phyllosilicate abundance up to 4.2 wt. % in CV_{OxB} (*vs.* 1.9 wt. % in Allende CV_{OxA}) through the determination of modal mineralogy by XRD diffraction. In Allende, hydrous phases are observed only in CAIs and chondrules, in low amounts (e.g., review by Krot et al., 1995). The main difference between CV_{OxB} and CV_{OxA}, based on the few studied CV chondrites, appears to be the much lower abundance of phyllosilicates in the latter (Krot et al., 1998a). In the matrix of CV_{Red} chondrites, phyllosilicates are less commonly observed than in CV_{OxB}. Saponite is observed in the matrix of Vigarano (based on TEM observations by Lee et al., 1996), and some phyllosilicate-rich rims (saponite and serpentine) around chondrules are also described (based on SEM-EDS and EPMA by Tomeoka and Tanimura, 2000). Incipient aqueous alteration in the matrix of Vigarano is also

indicated by the presence of oxyhydroxides such as ferrihydrite (Lee et al., 1996; Abreu and Brearley, 2011). Nevertheless, the degree of alteration of Vigarano appears to be variable. This might be related to the fact that Vigarano is a breccia containing CV_{OxA} and CV_{OxB} materials in addition to the CV_{Red} groundmass (Krot et al., 2000). Howard et al. (2010), limited by the detection limit of XRD diffraction method (~ 1 wt. %), did not identify any phyllosilicates in Vigarano and Efremovka CV_{Red}.

The secondary history experienced by chondritic parent bodies depends on a certain number of parameters. In particular for a given body, the total abundance of ^{26}Al (depending on e.g., the time and duration of the accretion, the size of the asteroid) and of ices played obviously a significant role in the thermal history and final hydration state (e.g., McSween et al., 2002). Among carbonaceous chondrites, a large range of relative intensity of metamorphism and aqueous alteration is observed reflecting a complex interplay between temperature and fluids. In particular, the temperatures that come into play on the parent bodies of type 3 chondrites are significantly higher ($\geq$ 300 °C) than for type 1 and 2 chondrites ($\leq$ 150 °C) (e.g., Brearley, 2006; Huss et al., 2006), the latter being characterized by a higher water on rock ratio (e.g. Marrocchi et al., 2018). As a result, in type 3 chondrites, the secondary anhydrous phases dominate over hydrous phases (e.g., Brearley, 2006) and a variety of secondary anhydrous phases (e.g., fayalite, sodalite, nepheline, magnetite…) are thereby commonly described in CV chondrites. Like phyllosilicates, nearly pure fayalite is common in CV_{OxB}, rare in CV_{Red}, and in even lower abundance in CV_{OxA} (review by Krot et al., 1995). A nebular origin has long been attributed to fayalite (e.g., Weinbruch et al., 1990). But it was later proposed that the formation of fayalite was the result of aqueous alteration or high-temperature metasomatism followed by dehydration on the CV asteroidal parent body (Krot et al., 1995;1998a;1998b; 2000). This mechanism was later questioned (e.g., Krot et al., 2004) mostly based on the lack of mass-dependent fractionation of oxygen isotopes (an

evidence for extensive hydration-dehydration) in contrast to the observations in metamorphosed type 1 and 2 chondrites (Clayton and Mayeda, 1999). Therefore, the growth of ferrous olivine (Fa_{40-100}) in the presence of limited quantities of aqueous fluid released during dehydration of phyllosilicates seems more likely than its direct formation from phyllosilicates (Krot et al., 2004; Abreu and Brearley, 2011).

The post-accretion history of CV chondrites is complex and debated (e.g., Krot et al., 1995; Brearley, 2003; Brearley and Krot, 2013). Although there is no consensus on the precise nature and specific products of secondary history (relative intensity of aqueous alteration, thermal metamorphism, and metasomatism), some general ideas emerge from the literature. Reduced and oxidized CV chondrites might have witnessed different physico-chemical conditions during post-accretional processes (e.g., Krot et al., 1998b; MacPherson and Krot, 2014). All CVs have experienced aqueous alteration, thermal metamorphism and metasomatism to variable extents. In particular, evidences of aqueous alteration are easily observed in CV_{OxB}, while CV_{OxA} primarily show evidence of metasomatism (Krot et al., 1995) and minimal evidence of aqueous alteration. In CV_{Red} chondrites, evidence for aqueous alteration appears to be minimal as well. Moreover, all CV chondrites experienced thermal metamorphism but remain non-equilibrated rocks, making it difficult to apply geothermometers to determine peak metamorphic temperatures. Nevertheless, several thermometers, with various significance, were applied to CV chondrites. In particular, a temperature range from 330 °C to 600 °C can be found through the literature for Allende alone (Rietmeijer and Mackinnon, 1985; Huss and Lewis, 1994; Busemann et al., 2007; Cody et al., 2008).

As abundant as the literature on CV chondrites might be, several limitations have to be underlined. *(i)* Somehow, most studies are focused on only one sample or at best on a few samples among Allende, Axtell, Grosnaja, Mokoia, Kaba, Leoville, Efremovka, and

Vigarano. Generalization to the CV parent body of observations on a single CV sample may be a bit bold. *(ii)* The understanding of the metamorphic history of CV chondrites has long been biased by the attribution of misleading petrologic types. For example, Allende has long been considered as a type 3.2 chondrite (Guimon et al., 1995), although it is actually the most metamorphosed chondrite among non-Antarctic CVs with a metamorphic type of ~3.7 (Bonal et al., 2006). *(iii)* The studied CV_{Red} chondrites Leoville, Vigarano and Efremovka span a limited metamorphic range between 3.1 and 3.4 (Bonal et al., 2006). This might induce some bias in terms of identification and interpretation of mineralogical properties related to secondary history and limit the reliability of comparison with CV_{Ox}. *(iv)* Allende is the only chondrite of CV_{OxA} subgroup that has been studied in details, making this subgroup poorly characterized. Indeed, Axtell, another CV_{OxA} chondrite, has not received as much attention, most likely because it is a weathered find (Simon et al., 1995).

In the present work, we study a set of 31 CV chondrites spanning a wide range of thermal metamorphism, through a combination of petrographic and mineralogical work, magnetic measurements, spectral and thermo-gravimetric analysis. The objective of this work is to better constrain the complex post-accretion history of CV chondrites, characterized by interplaying temperature and fluids.

2. SAMPLES AND ANALYTICAL METHODS

Petrographic observations on thin and/or thick sections, as well as measurements on matrix and bulk samples were performed on a series of 21 Antarctic and 10 non-Antarctic CV chondrites (Table 1).

2.1. Petrography

Metal modal abundances were determined by reflected light optical microscopy on polished sections by point-counting using a 500x magnification and a step size of 100 μm. The 95% confidence interval around the modal abundance was computed after Howarth (1998). A mosaic image of each section (reflected and/or transmitted light, using a 25x magnification) was used to determine the modal abundances of matrix and high-temperature components (chondrules, chondrule fragments, CAIs) through image analysis after manual contouring of individual high-temperature components down to a size of about 30 μm. The modal abundances of matrix in Bukhara and QUE 97186 were determined through point-counting and not image analyses, as the optical images were not of sufficient quality. Shock stages as defined by Scott et al. (1992) were determined for the Antarctic CV chondrites (except GRA 06101 for which no section was available).

2.2. Ni content of sulfides and metal grains

Nickel content of sulfides and Fe, Ni metal in Efremovka, Leoville, Vigarano, Allende, Mokoia, Kaba, Bali, and Grosnaja were previously published by McSween (1977). Additional analyses, in Antarctic chondrites mostly, were performed using either by wavelength dispersive spectrometry using an electron microprobe Cameca SX100 at CAMPARIS facility (15 kV accelerating voltage, 10 nA current), or using a Hitachi S3000-N Scanning Electron Microscope equipped with a Bruker X-ray Energy Dispersive Spectrometer at CEREGE. Both natural and synthetic standards were used for calibration (among which pure iron for Fe, pure nickel for Ni, pure cobalt for Co, pyrite for S).

2.3. Magnetic properties

All the magnetic measurements were performed at CEREGE (Aix-en-Provence, France). Magnetic susceptibility (χ) was measured using a MFK1 apparatus from Agico in an AC field

of 200 Am^{-1} (peak field) and frequency 976 Hz. Magnetic hysteresis properties were measured with a Princeton Micromag vibrating sample magnetometer (VSM) with a maximum applied field of 1 T. Hysteresis loops allowed the determination of saturation remanent magnetization (M_{RS}) and saturation magnetization (M_S). For the determination of M_S, paramagnetism and diamagnetism were corrected by linear fitting of the hysteresis cycle on the 0.9-1 T field interval. When multiple samples of the same meteorite were measured, M_{RS} and M_S were mass-weighted. A total of 106 samples were measured for hysteresis properties, with average, median, minimum and maximum mass of 238 mg, 78 mg, 8.5 mg, and 2.06 g, respectively. In addition we used the database of Rochette et al. (2008) for magnetic susceptibility measured in various collections on large samples, allowing to discuss the homogeneity of these meteorites. The three intrinsic magnetic properties (χ, M_S, M_{RS}) reflect the abundance of ferromagnetic minerals. In CV chondrites, these minerals can be any combination of magnetite, pyrrhotite, and a variety of Fe,Ni metallic minerals (kamacite, tetrataenite, awaruite). Only M_S is strictly proportional to the abundance of these minerals, with the following values for pure minerals: 92 Am^2kg^{-1} for magnetite, 24 Am^2kg^{-1} for pyrrhotite, 224 Am^2kg^{-1} for kamacite, 155 Am^2kg^{-1} for tetrataenite and 130 Am^2kg^{-1} for awaruite (Crangle and Hallam, 1963; Dunlop and Ozdemir, 1997; Gattacceca et al., 2014). M_{RS} and χ depend on the abundances of these minerals, but also on their magnetic grain size. This is especially true for M_{RS} which is highly sensitive to magnetic microstructures in Fe,Ni minerals (e.g., Gattacceca et al., 2014). These two parameters are thus more complex to interpret than M_S when mixtures of up to five ferromagnetic minerals are encountered, as in CV chondrites. At first order, χ is mostly controlled by magnetite and Fe,Ni minerals, whereas M_{RS} is more sensitive to the pyrrhotite and magnetite contents.

2.4. Transmission IR spectroscopy

Infrared (IR) spectra were obtained with a BRUKER HYPERION 3000 infrared microscope (IPAG, France). The IR beam was focused through a 15x objective and the typical size of the spot on the sample was 40 x 40 μm^2. Spectra were measured at 4 cm^{-1} spectral resolution with a MCT detector cooled with liquid nitrogen. Particular care was devoted to sample preparation, which is a critical issue in IR micro-spectroscopy. Samples must be thin (<100 μm) and their surfaces flat enough to avoid absorption-band saturation and scattering artifacts, respectively (e.g., Raynal et al., 2000). Small matrix fragments (30–50 μm) were selected under a binocular microscope according to their color and texture. The matrix fragments were crushed between two diamond windows, allowing access to the [4000 – 650] cm^{-1} spectral window. The diamond windows were loaded into an environmental cell, designed and built at IPAG. This cell enables temperatures of up to 300 °C to be reached under primary or secondary dynamic vacuum (from 10^{-4} mbar down to 10^{-7} mbar). Optical access is permitted from both sides of the cell through ZnS windows, thus enabling measurements in transmission. Samples were progressively heated up to 300°C, with typical steps at 100°C, 200°C, and spectra were recorded at each temperature step.

The transmission spectra were automatically converted to absorbance ($A = -\log (T/T_0)$, where T_0 and T are the transmittance without and with the sample, respectively). To remove interferences and scattering effects, a spline baseline was subtracted from the raw data.

2.5. Thermo-Gravimetric Analysis

TGA was used to quantify the amount of hydrogen in the samples by measuring the mass loss upon heating. The first derivative (DTG) of the TGA curve enables us to determine the maximum peak temperature of each mass loss and gives an indication of the host mineral of volatile elements (see Fig. 1 in Garenne et al., 2014). Thermo-Gravimetric measurements were performed with a TGA-DSC3 Mettler-Toledo at Institut des Sciences de la Terre

(ISTerre, Grenoble - France). A fragment of bulk sample was ground manually (around 50 mg in a mortar). 30 mg of this powder was extracted for TGA analysis and put inside a 150 µL alumina crucible under a 50 mL/min inert N_2 atmosphere. The mass loss from each sample was recorded as it was heated from 25 °C to 1000 °C with a heating rate of 10 °C/min. The TGA mass resolution is 1 µg, which corresponds to an absolute error of 0.7% for a total mass loss fraction of 5 %. The error on the temperature measurement is around 0.25 °C.

In comparison to Garenne et al. (2014) working on CM chondrites, the only additional standard we analyzed was saponite, as it was previously observed in CV chondrites (Tomeoka and Buseck, 1990; Keller and Buseck, 1990; Keller et al., 1994).

2.6. Raman spectroscopy

Raman spectra of matrix fragments from most CV chondrites considered in the present work were previously performed and interpreted in terms of metamorphic history by Bonal et al. (2006, 2016). Nevertheless, measurements were unsuccessful on a few Antarctic meteorites. High weathering grade of the bulk samples was indicated to explain the difficulty in obtaining a sufficient number of Raman spectra of exploitable quality. In the present work, measurements were made on thin section of ALH 84028, GRA 06130, LAR 06867, MIL 07002, and ALH 85006. This last CV chondrite was successfully previously characterized through Raman measurements on matrix fragments (Bonal et al., 2016). The comparison of the data obtained on sections *vs.* matrix fragments allows to assess the absence of analytical artifacts related to the sample preparation. The fall Bukhara is also an additional CV chondrite that was not previously characterized by Bonal et al. (2016). Last, although data were published by Bonal et al. (2016) on the raw sample, new measurements were performed on the section of MIL 07671 to check on the consistency of various parameters.

The Raman experiments were performed at Laboratoire de Géologie de Lyon (ENS Lyon – France) with a Labram spectrometer (Horiba-Jobin-Yvon) equipped with a Spectra Physics Argon ion laser and using 514.5 nm excitation. The experimental and analytical conditions were exactly the same as in Bonal et al. (2016) to allows the comparison.

3. RESULTS

3.1. Petrography and opaque minerals composition

Modal abundances of matrix and shock stages are given in Table 1. Matrix abundance is highly variable, ranging from 19.4 vol. % (in Efremovka) to 69.6 vol. % (in Grosnaja). Among the considered CV chondrites, shock stages vary between S1 and S4. Most of them have escaped significant shock and are characterized by shock stages S1 and S2.

The modal abundances of metal, and Ni contents in metal and sulfides minerals determined previously (McSween, 1977) and in the present work are reported in Table 2. Metal was observed in all studied meteorites, except Grosnaja. The abundances of metal (under the form of kamacite, tetrataenite, and awaruite) are highly variable among CV chondrites: metal is absent (Grosnaja), present as traces (e.g., in MCY 05219 and Axtell) or abundant (up to 4.60 vol. % in Efremovka). The average Ni contents of metal in the studied CV chondrites range between1.6 and 69.7 wt. %. The average Ni content in sulfides is also highly variable among the considered CV chondrites, ranging from 0 wt. % (e.g., in Efremovka) to 28.4 wt. % (in ALH 85006), spanning the range of troilite, pyrrhotite and pentlandite.

3.2. Intrinsic magnetic properties

Within a given CV3 chondrite, saturation remanent magnetization (M_{RS}), and saturation magnetization (M_S) are homogeneous at small scale, down to a sample size of a few dozen

mg. This is illustrated by the average intra-meteorite coefficients of variation of 18% for both M_{RS} and M_S. An intra-meteorite coefficient of variation of 15% can be computed for χ, based on the data obtained on larger samples (several grams scale) from Rochette et al. (2008).

In contrast with this intra-meteorite homogeneity, M_{RS} varies from ~ 17 to 2480 $x10^{-3}$ Am^2kg^{-1}, and M_S from ~ 90 to 18700 $x10^{-3}$ Am^2kg^{-1} among our series of 31 CV chondrites (Table 2). The overall inter-meteorite coefficient of variation is 99% for M_{RS} and 97% for M_S, respectively. This large range in magnetic properties is also reflected in the large range of magnetic susceptibility ($\log\chi$ from 3.10 to 4.85 in our dataset, with χ in 10^{-9} m^3kg^{-1}), already underlined by Rochette et al. (2008) based on measurements of 44 CV chondrites that indicate an inter-meteorite coefficient of variation of 138%. For comparison, H and L ordinary chondrites falls have inter-meteorites coefficients of variation of 17% and 34% for M_S, (computed after Gattacceca et al., 2014), and 23% and 15% for χ (computed after Rochette et al. (2003), respectively). This indicates highly variable abundances and mineralogy of ferromagnetic minerals among CV chondrites. This is consistent with pioneering observations by McSween (1977) stating a highly variable amount of metal and magnetite in CV chondrites.

3.3. Hydration – quantification of water and of secondary products

3.3.1. IR spectra

Each individual spectrum obtained on selected matrix fragments was baseline-corrected and then normalized to the maximum of the Si-O band (dominated by olivine). An average spectrum was then obtained for each considered CV chondrite. The IR spectra of matrix of each CV chondrite are characterized by the presence of bands related to water (broad feature ranging from 3650 to 3000 cm^{-1} + bending mode peaking at ~1650 cm^{-1}),

aliphatic bands (-CH_2, -CH_3), and Si-O stretching band centered around 1000 cm^{-1}, mostly related to olivine. A zoom on the 3-µm water band is shown on Fig. 1.

The success in selecting matrix fragments is proven by the presence of spectral bands, related to aliphatic organics, that are only present in the fine-grained chondritic matrix (e.g., Alexander et al., 2017). Several remarks can be made on the 3-µm water band observed on spectra acquired at 100 °C: *(i)* the matrix of each CV chondrite is hydrated, the hydration being variable; *(ii)* The water band is related to phyllosilicates and oxy-hydroxides. But the abundance of phyllosilicates is sufficiently low for them not being visible in the Si-O band, where olivine clearly dominates; *(iii)* the -OH band (stretching mode at ~3700 cm^{-1}) clearly visible on spectra of CI chondrites and related to the hydroxyl groups in phyllosilicate, is not easily seen on the spectra of CV chondrites, with the exception of Kaba.

IR spectroscopy is particularly sensitive to the presence of H_2O and –OH and allows the study of very small amounts of samples. The obtained spectra unambiguously reveal that CV chondrites are all hydrated, independently from their oxidation state. Nevertheless, the quantification of the water from these spectra is very difficult. Indeed, in transmission, the spectral intensity directly depends on the thickness of the sample and on the size of the analytical area. The spectra were thus normalized to the maximum intensity of the Si-O band to be independent from the thickness, potentially different for each sample preparation, and analytical area. But, depending on the metamorphic grade of the sample, the extent of its hydration, and also the exact mineralogy of the selected matrix fragment (potentially with more or less opaque minerals for example), the abundance of anhydrous silicate (and thus the intensity of the Si-O spectral band) might vary between samples. The normalization might then induce some error on the estimation of the water abundance. Moreover, the baseline correction might induce some biases, hardly controlled and quantifiable. The quantification of hydration was thus made through additional TGA measurements.

3.3.2. TGA

TGA were used to quantify the hydrogen budget of the meteorites (Table 3, Fig. SOM1). The DTG shows the variation of sample mass during heating (Fig. SOM1). The positions of the peaks as a function of temperature are characteristics of mineral groups at the first order (e.g., Garenne et al., 2014; King et al., 2015). However, the chemistry and crystallinity of minerals influence the exact temperature at which their water or hydroxyl will be released. The identification of specific minerals based on the DTG curves would thus require a dedicated study with the characterization and analysis of many standards. This was not our objective here, where we only use temperature ranges to quantify *(i)* abundances of the two main hydrous mineral phases (phyllosilicates *vs.* oxy-hydroxides) and, *(ii)* the total mass loss to quantify the global dehydration and dehydroxylation of each sample (Table 3).

The mass loss curves were decomposed into distinct temperature ranges: [< 200°C], [200 – 350 °C], and [350 – 850 °C] (Fig. SOM1). The first part of the mass loss curve, from 25 to 200 °C, corresponds to the release of weakly bonded water from adsorption or chemisorption. Due to the potentially large contribution of ambient terrestrial water, this low-temperature region of the TGA curve is not exploited. Only the mass loss measured at T > 200 °C is here considered. The second part of mass loss between 200 and 350 °C is attributed, at first order, to the release of H_2O from (oxy)-hydroxide minerals. The third part, from 350 to 850 °C, is assigned to the dehydration and dehydroxylation of phyllosilicates and to the decomposition of iron sulfides. Indeed, iron sulfides (pyrite, pyrrhotite, troilite and mixtures) decompose between 400 and 650°C (e.g., Garenne et al., 2014; King et al., 2015). Because they are strongly oxidative and because of their complicated oxidation behavior, the investigation of sulfide minerals by TGA is quite difficult (Földvári, 2011). In particular, pure pyrrhotite appears to lose ~30% of its mass between 200 and 900 °C, while a mixture of pentlandite and

pyrrhotite is characterized by a much lower mass loss (~ 10 wt. %) (Garenne et al., 2014). Sulfides in CV chondrites are mostly pyrrhotite and pentlandite, but with specific relative abundances not determined here. To precisely retrieve the contribution of sulfides decomposition to the total mass loss, a systematic TGA study of pure and mixtures of sulfides would be required, in addition to a dedicated mineralogical work. This is beyond the scope of the present paper. However, considering the average abundance of sulfides in CVs (2.2 vol. % *i.e.* 3.5 wt. %; n = 8; McSween, 1977) and an approximate mass loss of 10 wt. % due to the higher abundance of pentlandite in comparison to pyrrhotite, the mass loss induces by sulfides is around 0.35 wt. %. We thus note that the presence of sulfides could lead to a slight over-estimation (~ 0.35 wt. %) of the total water content.

The semi-quantification based on IR spectral features of the 3-µm band is poorly correlated ($r^2 = 0.33$) to the total hydration as estimated through TGA measurements (Fig. SOM2). This result is not surprising considering the difficulties of quantification through IR spectroscopy (see §3.3.1).

Carbonates are secondary minerals related to the aqueous alteration experienced by meteorites on their parent bodies (e.g., Brearley, 2006). As carbonates are not hydrated, they will not contribute to the H budget through dehydration or dehydroxylation upon heating of the samples. However, they typically decompose at temperatures between 600 – 900°C (Nozaki et al., 2006; Nakato et al., 2008; Garenne et al., 2014; King et al., 2015), the exact temperature being influenced by the chemical composition of each carbonate, but also by the grain size of the sample (Garenne et al., 2014). Nevertheless, the abundance of carbonates in CV chondrites is low: indeed, carbonates are not detected by X-ray diffraction in Vigarano, Efremovka, Mokoia, Grosnaja, Kaba and Allende, the abundance is thus lower than 1 wt. % (Howard et al., 2010) and no specific thin peak characteristics of carbonates were observed on

the DTG curves for temperatures > 600°C. The contribution of carbonates to the total mass loss is thus negligible.

Terrestrial weathering strongly affects TGA results by the decomposition of e.g., terrestrial oxyhydroxides and/or carbonates. Therefore, these data cannot be used as a reliable proxy of parent body hydration.

3.4. Terrestrial weathering

All meteorites collected in Antarctica are finds, with average terrestrial ages 99 ka computed on 398 ages extracted from MetBase database (Koblitz, 2005). Even though terrestrial weathering is slower in cold than in hot deserts (Bland et al., 2006), the exposure to terrestrial conditions is not without consequences. In particular, ferruginous oxidation products are the most obvious weathering products in meteorites (Bland et al., 2006): a suite of oxides and oxyhydroxides has indeed been reported in ordinary and carbonaceous chondrites (e.g, Bland et al., 2006; Munayco et al., 2013). It is thus possible that some ferrihydrite results from terrestrial weathering in our samples (Abreu and Brearley, 2011). However, the correlation observed between the low-temperature mass loss and the peak metamorphic temperature (see § 4.4) suggests that most oxyhydroxides present in our samples are related to extraterrestrial alteration. Abreu and Brearley (2005) also revealed a variable abundance of calcite in two separate stones of Vigarano, with in particular its common presence as veins, interpreted as terrestrial in origin, in the stone recovered one month after the observed fall. Terrestrial weathering can also lead to strong changes in the magnetic properties of metal-bearing meteorites (Rochette et al., 2003, 2008; Uehara et al., 2012). A few of the Antarctic chondrites considered here, or at least the samples we had for analysis, have been significantly weathered on Earth. *(i)* QUE 94688 is characterized by an excess in water released under 200°C during TGA measurements (Table 3). Moreover, the peak

position on the DTG curve for goethite is distinct from that of other oxy-hydroxides (Garenne et al., 2014; King et al., 2015) and was firmly identified in QUE 94688. Lastly, the section is lacking opaque minerals, as they all appear to be corroded in reflected light microscopy (Fig. SOM3). *(ii)* LAR 06867 is also characterized by an excess of water released under 200°C and by a total mass loss and total hydration [200 – 900 °C], particularly high in comparison to the other chondrites (Table 3). A majority of the opaque minerals are corroded as well (Fig. SOM3). *(iii)* GRO 95652 is characterized by an excess in water released under 200°C during TGA measurements (Table 3) and although some metal grains are still visible in polished section, a large majority of them are corroded (Fig. SOM3). *(iv)* Goethite is identified in MIL 091010, based on magnetic measurements and terrestrial weathering is clearly visible through optical microscopy (Fig. SOM3). Moreover, Axtell is known to be weathered (e.g., Simon et al., 1995), consistent with a high total mass loss (Table 3) and the presence of corroded opaques (Fig. SOM3).). It is also the CV meteorite showing the lowest M_S combined with 0 vol. % modal abundance of metal. Only QUE94688 shows a lower magnetic susceptibility logχ. Interestingly, Bukhara is characterized by a high ratio between the low- and the high-temperature mass loss (Table 3). Based on our petrographic observations of the thin section, metal is perfectly preserved. However, under the binocular the bulk sample that was allocated to us appears very bright and with a whitish color, typical of weathered samples. Although Bukhara is a fall from 2001, this particular sample may have experienced significant terrestrial weathering leading to the formation of oxyhydroxides.

3.5. Metamorphic history

Raman spectra of the polyaromatic carbonaceous matter present in CV chondrites were previously acquired by Bonal et al., (2006, 2016) on selected matrix fragments. We complement this dataset with measurements on six additional CV chondrites. Indeed, in the

previous study, spectral acquisition was unsuccessful on a few chondrites, for which a high weathering grade was pointed out (Bonal et al., 2016). The *in situ* acquisition of Raman spectra is usually not the favored method due to potential presence of epoxy mixed with the fine-grained and porous matrix due to impregnation during sample preparation. Epoxy might in some case induced the superimposition of a fluorescence background on the Raman signal from the chondritic carbonaceous matter. However, this issue does not systematically occur with thin or polished sections, as it directly depends on the epoxy used, the sample preparation, and the sample porosity. In the present case, no interfering fluorescence signal was observed. Moreover, it was previously noted that the structural order of the surface layer of carbonaceous matter could be modified during sample polishing (Beyssac et al., 2003), depending on the maturity of this carbonaceous matter. In the case of type 3 chondrites, no modification of the structural order induced by polishing is observed, as previously discussed by Bonal et al. (2016) and confirmed here by the totally comparable parameters obtained for ALH 85006 either on thin section or selected matrix fragments (Table 4).

Spectral parameters of MIL 07671 published by Bonal et al. (2016) identified it as a 3.1 chondrite. However, the lack of consistency with the set of parameters obtained in the present study led us to perform a new Raman characterization on the section of MIL 07671. The obtained results are inconsistent with the previous ones done on bulk matrix fragments: MIL 07671 is metamorphosed with a petrologic type of 3.7. We interpret this discrepancy as stemming from a sample mislabeling in the previous study.

All CV chondrites studied in the present paper by Raman spectroscopy (LAR 06867, ALH 84028, GRA 06130, MIL 07002, MIL 07671 and the Bukhara fall) have a petrologic type of at least 3.6 (Table 4).

4. DISCUSSION

The following discussion is based on a series of 31 CV chondrites, including 7 falls, 21 meteorites from Antarctica, and 3 non-Antarctic finds (Table 1). This is the first time that such a large set of meteorites is used to assess the history of the CV chondrite parent body.

4.1. Potentially paired samples

Pairing Antarctic meteorites is not an easy task (e.g., Benoit et al., 2000). Pairing suggestions are based mostly on petrography, geographical proximity and weathering. None of the considered Antarctic meteorites considered here are listed as paired in the Antarctic Meteorite Newsletter nor in the Meteoritical Bulletin. However, based on similar experienced post-accretion histories and magnetic properties, we suggest here MET 00430, MET 00671, and MET 01074 to be paired (assumption consistent with them being aligned along approximately 6 km, based on GPS coordinates from John Schutt). Indeed, it was shown that the magnetic susceptibility is a good tracer to define affinities among carbonaceous chondrites and to propose pairing (Rochette et al., 2008). MET 00430, MET 00671 and MET 01074 all have $\log\chi$ = 4.69, strengthening the pairing hypothesis (Table 5). The Raman spectral parameters describing the structural order of their polyaromatic carbonaceous matter are also similar (Table 5), reflecting a comparable thermal history. The high-temperature mass loss, the least sensitive to potential terrestrial weathering, is also similar among these three MET CV chondrites, reflecting a comparable hydration. Same observations can be done for MIL 07002 and MIL 07671 that are most likely paired. In the other hand, MIL 07277 and MIL 091010 are characterized by too diverse petrography, magnetic properties and thermal history to be paired samples.

4.2. Classification of CV chondrites into CV_{OxA}, CV_{OxB}, CV_{Red}

Subclassification of CVs has been defined in the literature to reflect the petrographic diversity of that chondrite group. In particular, CV_{Red} and CV_{Ox} were originally distinguished based on the modal abundances of metal and magnetite and on the Ni contents of sulfides and metal mostly (McSween, 1977). Moreover, it was also previously noted by McSween (1977), based on a series of 8 CVs that the matrix/chondrules ratios fall into two distinct groups (a third group was originally defined by the Coolidge meteorite, now classified as a C4 chondrite). Although they were not exactly coinciding with the oxidized-reduced subdivisions, it was concluded that CV_{Ox} tend to be enriched in matrix compared to CV_{Red}, which was later confirmed by Weisberg et al. (1997). CV_{Ox} were then subdivided into Allende-like (CV_{OxA}) and Bali-like (CV_{OxB}) in an abstract by Weisberg et al. (1997). The subgroups were later more precisely defined by Krot et al. (1998) and have been commonly used in the literature since then. Because they were based on a small number of samples, the distinct quantitative parameters that were considered (i.e., matrix/chondrules, metal/magnetite ratios, iron content of fayalitic olivine in matrix, variable abundance of phyllosilicates) were not statistically significant. Moreover, they tend to overlap, preventing a fully straightforward sub-classification of CV chondrites. In the present work, one of our objectives was *(i)* to decipher whether a subclassification of oxidized CV chondrites into CV_{OxA} and CV_{OxB} is justified and *(ii)* if justified, determine quantitative parameters to firmly define the subclassification CV_{Red} *vs.* CV_{OxA} *vs.* CV_{OxB}.

Petrographic classification into oxidized and reduced subgroups on Antarctic CV chondrites had not been done systematically so far, and only a few samples were classified in the literature. We classified the 31 studied CV chondrites into the CV_{OxA}, CV_{OxB} and CV_{Red} sub-groups based on the modal abundance of metal (with a cut-off value at about 1 vol. % metal) and the average Ni content of sulfides (with a cut-off value at 3 wt. % Ni). Some overlap between CV_{OxA} and CV_{OxB} was resolved using the abundance of magnetite estimated

through saturation magnetization M_s. The proposed classification is given in Table 6. ALHA 81003, ALH 84028, and ALH 85006 were previously classified as oxidized by Krot et al. (1995) based on qualitative estimates of modal abundances of opaque minerals, in agreement with the present work. LAR 06317 was classified as CV_{OxA} by Lunning et al. (2016), while we classify it as CV_{OxB}. Classification of RBT 04143 as CV_{Red} is consistent with Ishida et al. (2012) and Lunning et al. (2016), but inconsistent with Wasson et al. (2013). We agree with Ishida et al. (2012) on the classification of QUE 97186 as CV_{Red} and of LAP 02206 and GRA 06101 as CV_{OxA}, and with Wasson et al. (2013) on the classification of MIL 07002 as CV_{OxA}. Our classification thus agrees with most classifications done earlier.

Based on our series of 31 samples, we do confirm the petrographic diversity of the CV chondrite group: abundances of matrix, as well as the nature and abundance of opaque minerals are highly variable (Tables 1 and 2). CV_{Red} have lower abundance of matrix than CV_{Ox} (Fig. 2a), higher abundance of metal (Fig. 2a), and contain Ni-poor metal and sulfides (Fig. 2b, 2d). CV_{OxA} and CV_{OxB} are not readily distinguished with these criteria. Indeed, CV_{OxA} and CV_{OxB} are characterized by similar matrix abundances (Fig. 2a). Although the metal abundance tends to be lower in CV_{OxB} than in CV_{OxA} (Fig. 2a, 2c), this single parameter does not allow to distinguish the two subgroups. On the other hand, the Ni content of metal (when metal grains are indeed present, Fig. 2b), the saturation remanence (Fig. 2c) and magnetic susceptibility (Table 6) unequivocally separate CV_{OxA} from CV_{OxB}. The combination of these parameters (Fig. 2, Table 7) justifies the subclassification into CV_{OxA}, CV_{OxB}, and CV_{Red}, as summarized in Table 6, where individual and average quantitative relevant parameters are reported.

4.3. Total hydration *vs.* thermal metamorphism experienced by CV chondrites

The total mass loss between 200 and 900 °C is highly variable and at most 4.5 wt. % in bulk CV chondrites (Table 3) while in CM and CI chondrites it is up to three times higher (Garenne et al., 2014; King et al., 2015). CV3 chondrites are not dry, but significantly less hydrated than type 1 and type 2 chondrites.

There is a general trend observed between the total mass loss and the Raman spectral parameter $FWHM_D$ (Fig. 3a): the hydration tends to decrease with decreasing $FWHM_D$. The maturity of polyaromatic carbonaceous matter is controlled by the metamorphic conditions (pressure, time, temperature, etc.) and the initial structure and composition of the organic precursors. In type 3 chondrites, it was previously shown that the maturation of the polyaromatic carbonaceous matter is mostly controlled by the peak metamorphic temperature (see discussion in Bonal et al., 2016). Hence the spectral parameter $FWHM_D$ is considered here as reflecting the peak metamorphic temperature experienced by a given chondrite. In other words, the trend observed between the TGA and Raman data indicates that the total hydration measured in bulk CV chondrites tends to decrease with an increasing peak metamorphic temperature. Nevertheless, the data appear to be quite scattered along this general trend, with in particular CV_{Red} that appear less hydrated than CV_{Ox} (Fig. 3a). The fine-grained porous matrix is highly sensitive to post-accretion processes and it is the first component to become hydrated through interaction with a fluid. The modal abundance of matrix varies from 19.4 to 69.6 vol. % among the studied CV chondrites (Table 1) and on average CV_{Red} contain less matrix than CV_{Ox} (50.4 *vs.* 35.1 vol. %, respectively, Table 5), as previously noticed by McSween (1977) and Weisberg et al. (1997). Although some chondrules and refractory inclusions contain some hydrated products (e.g., Cohen et al., 1983; Tomeoka and Buseck, 1990; Keller and Buseck, 1990; Keller et al., 1994; Brearley, 1997; Kimura and Ikeda, 1998), normalizing the total mass loss measured in a bulk sample to the abundance of matrix counterbalances large differences in matrix abundances. When

considering the total mass loss normalized to matrix abundance of each sample, the trend between the hydration and the peak metamorphic temperature appears more clearly (Fig. 3b).

Although a majority of the CV chondrites considered here are finds (Table 1; note that we have not included any finds from hot deserts in our study), the obvious effects of terrestrial weathering are limited to a few samples: QUE 94688, LAR 06867, MIL 091010, GRO 95652, and Axtell (see §3.4). These are specifically the samples that fall off the trend "hydration *vs.* peak metamorphic temperature" (Fig. 3b): they appear to be enriched in water and hydrated minerals in comparison to samples characterized by similar metamorphic grade (i.e., similar $FWHM_D$). As terrestrial weathering has overprinted the parent body hydration of these samples, these meteorites will not be further considered in the discussion.

Finally, with the exception of particularly weathered samples, and considering the individual matrix abundances, a clear trend appears between the total hydration and the peak metamorphic temperature experienced by CV chondrites (Fig. 3b): *(i)* the total hydration of bulk CV chondrites is anti-correlated to the experienced peak metamorphic temperature; *(ii)* the total hydration is independent from the subclassification: the matrix of CV_{Ox} and CV_{Red} meteorites are equally hydrated for a given metamorphic grade; *(iii)* CV_{OxA} are systematically more metamorphosed and therefore less hydrated than CV_{OxB}.

A trend with $FWHM_D$ (cm^{-1}) is also observed when considering the TGA high-temperature mass loss (Fig. 5a), indicating that the abundance of phyllosilicates decreases with increasing peak metamorphic temperature. Last, a trend, although less robust, is also observed between the TGA low-temperature mass loss and $FWHM_D$ (cm^{-1}): it first decreases with $FWHM_D$ down to ~115 cm^{-1} and then plateau for lower values of $FWHM_D$ (Fig. 5b). Oxyhydroxides, notably ferrihydrite, are low temperature alteration products (forming below 150 °C; e.g., Dehouck et al., 2017) that may crystallize during retrograde metamorphism on the parent body and/or during terrestrial weathering (Abreu and Brearley, 2011).

Nevertheless, the broad relation between the low-temperature mass loss and $FWHM_D$ > 115 cm^{-1} (Fig. 5b) strongly suggests that *(i)* oxyhydroxides are mostly parent body products and not formed through weathering on Earth, and *(ii)* their abundance is controlled by the peak metamorphic temperature. For $FWHM_D$ < 115 cm^{-1}, oxyhydroxides might either be thermally decomposed or not formed in higher abundance due to the limited quantity of aqueous fluids available during retrograde metamorphism.

4.4. Interplay between aqueous alteration and thermal metamorphism

Rubin (2012) proposed that the variable extent of alteration in CV chondrites could be explained by considering matrix porosities, compaction and fracturation, related to impacts. This is based in particular, on the observation that the CV_{Red} (characterized by low porosity) and CV_{OxB} samples (with higher porosity) tend to have petrofabrics while the CV_{OxA} (porosity similar to CV_{OxB}) samples do not, interpreted as reflecting how much water seep into them to facilitate alteration. However, based on a larger set of samples, these observations are no longer valid: there is no correlation between the total hydration and the shock stages within CV chondrites, and our petrographic observations do not confirm that CV_{Red} and CV_{OxB} have a more developed petrofabric than CV_{OxA}. One can then envision two main scenarios to explain the relationship between the final hydration state and the peak metamorphic temperature: *(i)* variable initial abundance of water ice (acting as a thermal buffer) in the matrix of CV chondrites; *(ii)* homogeneous initial abundance of water in the matrix, with the extent of current hydration of the matrix controlled by the peak metamorphic temperature.

The first scenario is advocated by some authors to explain the divergent thermal history of type 1 and 2 *vs.* type 3 carbonaceous chondrites (e.g., Grimm and McSween, 1989). If we hypothesize an initially homogenous mixture of ice and rock, the amount of water should be proportional to the abundance of matrix. Considering the large latent heat of fusion of ice, the

high heat capacity of water and the heat loss through water circulation, one might expect the chondrites that are the richest in matrix (i.e., the one having experienced the most interaction with water on the asteroidal parent body) to be the least heated. However, this is not what we observe here: the CV chondrites characterized by the highest abundance of matrix are not the ones having experienced the lowest peak metamorphic temperatures (Fig. 4). Therefore, the higher hydration of CV chondrites having experienced lower peak metamorphic temperature (Fig. 3b) cannot be explained by water ice acting as a thermal buffer.

In the second scenario, there is no heat mitigation by the buffering effects of water. The CV3 parent body was thus *gradually* heated through the radioactive decay of ^{26}Al. Upon reaching the melting temperature of ice, soon after accretion (e.g., Jogo et al., 2017), aqueous alteration was initiated. Formation of secondary minerals occurred over an extended time period of most likely several millions of years (e.g., Brearley, 2006). This does not necessarily reflect a continuous process, as aqueous alteration could have been episodic (e.g., Brearley, 2006). Thermal metamorphism and aqueous alteration are not necessarily conjoint processes as the internal temperature could have continued to increase up to the peak metamorphic temperature after exhaustion of the reservoir of ice (after aqueous alteration ceased). Peak metamorphic temperatures are not unequivocally established in CV3 chondrites, but have been most likely as high as several hundreds of °C (e.g., Huss et al., 2006; Brearley and Krot, 2013). Hydrated secondary minerals might have thus experienced *(i)* subsequent dehydration or *(ii)* degradation through heating. In the most thermally metamorphosed chondrites, one could also imagine that the formation of hydrated secondary minerals was limited by the rapid exhaustion of water through heat and the associated kinetic inhibition of hydration reactions. A water to rock ratio lower in CV_{OxA} than in CV_{OxB} due to water being driven off by high temperatures was previously suggested by Greenwood et al. (2010) to explain different oxygen isotopic compositions. The dehydration scenario or limited

hydration reactions easily explain the lower hydration observed in the most thermally processed CV chondrites (Fig. 3b). Oxyhydroxides have a lower thermal stability than phyllosilicates, explaining why above a certain peak metamorphic temperature (i.e., for $FWHM_D$ < ~120 cm^{-1}), the low-temperature mass loss is low and constant (Fig. 5b), while the high-temperature mass loss decreases along the whole range of peak metamorphic temperatures (Fig. 5a). Moreover, in the CV chondrites that have experienced mild peak metamorphic temperatures ($FWHM_D$ < ~120 cm^{-1}), enough aqueous fluids may have been still available to form oxyhydroxides during retrograde thermal metamorphism. The dehydration or limited hydration scenario is not easily reconciled with the one proposed by Ganino and Libourel (2017), with crystallization of secondary Ca-, Fe-rich anhydrous minerals before the formation of hydrous phases during low-temperature part of fluid-assisted thermal metamorphism.

4.5. Alteration products and opaque minerals in CV_{OxA}, CV_{OxB} and CV_{Red}

We showed here that CV chondrites (CV_{Red} and CV_{Ox}) are hydrated to a variable extent that is controlled by the peak metamorphic temperature. Based on the total hydration normalized to matrix abundances, it is not possible to distinguish CV_{Red} from CV_{Ox}. Nevertheless, CV_{Red} and CV_{OxB} appear to be characterized by distinct relative abundances of secondary hydrated products. Indeed, the comparison of low- and high-temperature mass loss estimated through TGA ([200 – 350 °C] and [350 – 900 °C], respectively) reveals that (Fig. 6): *(i)* the mass losses over the two temperature ranges are roughly correlated; *(ii)* CV_{Red} tend to be enriched in low-temperature alteration products (i.e., abundance of oxy-hydroxides) in comparison to CV_{OxB}. Moreover, abundance of metal and magnetite, as reflected by point counting and saturation magnetization M_S, are highly variable among CV chondrites (Table 2). CV_{OxA} are systematically depleted in magnetite and metal. Their average $M_S = 0.69 \pm 0.37$

Am^2kg^{-1} (Table 6) indicates maximum magnetite and metal content well below 1 wt. %. In contrast, CV_{OxB} contain abundant magnetite and CV_{Red} abundant magnetite and metal. Their saturation magnetization values (average Ms = 5.44 ± 3.01 Am^2kg^{-1} for CV_{OxB}, M_S = 8.47 ± 4.43 Am^2kg^{-1} for CV_{Red}, Table 6) indicate an average content of about 6 wt. % of magnetite in CV_{OxB} (neglecting the contribution of pyrrhotite to M_S, see §2.3), and several wt. % of both metal and magnetite in CV_{Red}. Nevertheless, it appears that above a given peak metamorphic temperature ($FWHM_D$ < 80 cm^{-1} i.e. metamorphic grade comparable or higher to that of Axtell (>3.6)), the total abundance of magnetite and metal clearly drops (M_S is systematically lower than 2 $A.m^2.kg^{-1}$ for $FWHM_D$ < 80 cm^{-1}, Fig. 7a). However, the total abundance of iron appears to be quite homogeneous among CV chondrites, with an average of 22.64 ± 0.85 wt.% (n=13) (Jarosewich, 1990; Wasson et al., 2013; Braukmüller et al., 2018), revealing closed-system conditions of post-accretion processes at the scale of a meteorite (~ decimeter scale). As the abundance of ferromagnetic minerals drops once a certain temperature is reached, the iron might be redistributed into non-ferromagnetic minerals such as fayalite or specific metallic phase. Interestingly, although CV_{OxA} contain less ferromagnetic minerals than CV_{OxB} (Table 2, Fig. 7a), they do contain on average more metal than CV_{OxB} (Table 5, Fig. 7b). Except in Allende, in which 3 out of 26 analyzed metal grains have compositions in the kamacite and tetrataenite range (McSween, 1977), all metal in the studied CV_{OxA} has a Ni content in the range 64 - 70 wt.% with an average of 67.3 ± 0.7 wt.% (n = 8) excluding Allende (Table 5), very close to $FeNi_3$ (awaruite). Regardless of the small numbers of analyzed grains, this was checked thoroughly by qualitative EDS observations. The Fe,Ni phase diagram (e.g., Yang et al., 1997) shows that awaruite cannot be formed by cooling from any initial Fe,Ni composition that is close to solar composition of about 10 wt.% Ni. Instead, forming awaruite by slow cooling requires starting composition of at least 68 wt.% Ni. Awaruite is clearly a secondary hydrothermal mineral and indeed it is a common trace

mineral in terrestrial serpentinite (e.g., Sleep et al., 2004). This conclusion is contrasting with the scenario of nebular formation for the awaruite in some Allende chondrules (Rubin, 1991). In CV_{Ox} chondrites, awaruite is found exclusively in the CV_{OxA} sub-group, another indication that this sub-group has suffered more intense hydrothermalism. In contrast the Fe,Ni metal of CV_{Red} and CV_{OxB} chondrites consists mostly of kamacite (McSween et al., 1977) and is a primary nebular product. It is noteworthy that the occasional kamacite found in Allende CV_{OxA} is restricted to the interior of chondrules (Clarke et al., 1971) where it has been preserved from hydrothermalism.

Distinct alteration products in CV_{Ox} and CV_{Red} had been previously underlined by Lee et al. (1996). These authors suggested that this difference in hydrated and hydroxylated alteration products might be explained by distinct water to rock ratios that responded more or less completely to change in redox conditions consistent with Ganino and Libourel (2017). However, although CV_{Ox} and CV_{Red} have distinct matrix abundances, CV_{OxA} and CV_{OxB} have similar matrix abundances (Table 5). Moreover, in comparison to CV_{OxB}, CV_{OxA} are systematically *(i)* more metamorphosed (Fig. 3b), *(ii)* less hydrated (Fig. 3b), *(iii)* depleted in ferromagnetic minerals (Fig. 7a), *(iv)* but enriched in metal in the form of secondary awaruite (Fig. 7b). CV_{OxB} chondrites are thus good candidates as the precursor material for CV_{OxA} chondrites. In other words, CV_{OxA} may be thermally metamorphosed CV_{OxB}.

5. CONCLUSION

CV chondrites are petrographically diverse (e.g., variable abundances of matrix and ferromagnetic minerals) and have experienced a complex post-accretion history. In the present work, we defined specific quantitative tracers to distinguish CV_{OxA}, CV_{OxB} and CV_{Red}, and constrain their post-accretion history, with the objective to clarify the role played by both

water and heat to shape the final meteorites. The principal conclusions of our work are the following:

1. CV_{OxA}, CV_{OxB}, and CV_{Red} experienced aqueous alteration. The three subgroups contain oxyhydroxides and phyllosilicates.
2. The degree of hydration observed today in individual CV chondrite is controlled by the experienced peak metamorphic temperature. Some reduced CV chondrites are as hydrated as oxidized CV chondrites.
3. CV_{OxA} are less hydrated than CV_{OxB}. CV_{OxA} may be thermally metamorphosed CV_{OxB}.
4. CV_{Red} are significantly distinct from CV_{Ox} in terms of matrix abundances, alteration products (relative abundances of oxyhydroxides and phyllosilicates), and opaque mineralogy. This could be indicative of a single heterogeneous CV parent body or of the sampling of distinct parent bodies.

Acknowledgements

US Antarctic meteorite samples are recovered by the Antarctic Search for Meteorites (ANSMET) program which has been funded by NSF and NASA, and characterized and curated by the Department of Mineral Sciences of the Smithsonian Institutions and Astromaterials Acquisition and Curation Office at NASA Johnson Space Center. We acknowledge sample loans from the Field Museum (Chicago, IL), the Natural History Museum (London), and the Museum d'Histoire Naturelle (Paris). We also thank Kevin Righter and John Schutt for answering our questions regarding pairing of Antarctic meteorites. This work has been funded by the Centre National d'Etudes Spatiales (CNES–France). The Raman facility in Lyon is supported by the Institut National des Sciences de l'Univers (INSU–France). We thank two anonymous reviewers, Dr. Adrian Brearley and Dr. Sasha Krot (Assistant Editor) for their careful reviews and relevant comments.

BIBLIOGRAPHY

Abreu N. M. and Brearley A. J. (2005) Carbonates in Vigarano: Terrestrial, preterrestrial, or both? *Meteoritics & Planetary Science* **40**, 609–625.

Abreu N. M. and Brearley A. J. (2011) Deciphering the nebular and asteroidal record of silicates and organic material in the matrix of the reduced CV3 chondrite Vigarano: Matrix in the CV3 chondrite Vigarano. *Meteoritics & Planetary Science* **46**, 252–274.

Alexander C. M. O., Cody G. D., De Gregorio B. T., Nittler L. R. and Stroud R. M. (2017) The nature, origin and modification of insoluble organic matter in chondrites, the major source of Earth's C and N. *Chemie der Erde - Geochemistry* **77**, 227–256.

Amelin Y., Kaltenbach A., Iizuka T., Stirling C. H., Ireland T. R., Petaev M. and Jacobsen S. B. (2010) U–Pb chronology of the Solar System's oldest solids with variable 238U/235U. *Earth and Planetary Science Letters* **300**, 343–350.

Benoit P. H., Sears D. W. G., Akridge J. M. C., Bland P. A., Berry F. J. and Pillinger C. T. (2000) The non-trivial problem of meteorite pairing. *Meteoritics & Planetary Science* **35**, 393–417.

Beyssac O., Goffé B., Petitet J.-P., Froigneux E., Moreau M. and Rouzaud J.-N. (2003) On the characterization of disordered and heterogeneous carbonaceous materials by Raman spectroscopy. *Spectrochimica Acta Part A: Molecular and Biomolecular Spectroscopy* **59**, 2267–2276.

Bland P. A., Zolensky M. E., Benedix G. K. and Sephton M. A. (2006) Weathering of chondritic meteorites. In *Meteorites and the Early Solar System II* D.S. Lauretta and H.Y. McSween Jr. pp. 853–867.

Bonal L., Quirico E., Bourot-Denise M. and Montagnac G. (2006) Determination of the petrologic type of CV3 chondrites by Raman spectroscopy of included organic matter. *Geochimica et Cosmochimica Acta* **70**, 1849–1863.

Bonal L., Quirico E., Flandinet L. and Montagnac G. (2016) Thermal history of type 3 chondrites from the Antarctic meteorite collection determined by Raman spectroscopy of their polyaromatic carbonaceous matter. *Geochimica et Cosmochimica Acta* **189**, 312–337.

Braukmüller N., Wombacher F., Hezel D. C., Escoube R. and Münker C. (2018) The chemical composition of carbonaceous chondrites: Implications for volatile element depletion, complementarity and alteration. *Geochimica et Cosmochimica Acta* **239**, 17–48.

Brearley A. J. (1997) Disordered Biopyriboles, Amphibole, and Talc in the Allende Meteorite: Products of Nebular or Parent Body Aqueous Alteration? *Science* **276**, 1103–1105.

Brearley A. J. (2003) Nebular versus Parent-body Processing. In *Treatise on Geochemistry* Elsevier. pp. 247–268.

Brearley A. J. (2006) The action of water. In *Meteorites and the Early Solar System II* D.S. Lauretta and H.Y. McSween Jr., Tucson. pp. 584–624.

Brearley A. J. and Krot A. N. (2013) Metasomatism in the Early Solar System: The Record from Chondritic Meteorites. In *Metasomatism and the Chemical Transformation of Rock* Springer Berlin Heidelberg, Berlin, Heidelberg. pp. 659–789.

Busemann H., Alexander M. O. and Nittler L. R. (2007) Characterization of insoluble organic matter in primitive meteorites by microRaman spectroscopy. *Meteoritics & Planetary Science* **42**, 1387–1416.

Clarke R. S. J., Jarosewich E., Mason B., Nelen J., Gomez M. and Hyde J. R. (1971) The Allende, Mexico, Meteorite Shower. *Smithsonian Contributions to the Earth Sciences* **5**, 1–53.

Clayton R. N. and Mayeda T. K. (1999) Oxygen isotope studies of carbonaceous chondrites. *Geochimica et Cosmochimica Acta* **63**, 2089–2104.

Cody G. D., Alexander C. M. O., Yabuta H., Kilcoyne A. L. D., Araki T., Ade H., Dera P., Fogel M., Militzer B. and Mysen B. O. (2008) Organic thermometry for chondritic parent bodies. *Earth and Planetary Science Letters* **272**, 446–455.

Cohen R. E., Kornacki A. S. and Wood J. A. (1983) Mineralogy and petrology of chondrules and inclusions in the Mokoia CV3 chondrite. *Geochimica et Cosmochimica Acta* **47**, 1739–1757.

Crangle J. and Hallam G. C. (1963) The magnetization of face-centred cubic and body-centred cubic iron + nickel alloys. *Proceedings of the Royal Society of London. Series A. Mathematical and Physical Sciences* **272**, 119–132.

Dehouck E., McLennan S. M., Sklute E. C. and Dyar M. D. (2017) Stability and fate of ferrihydrite during episodes of water/rock interactions on early Mars: An experimental approach: Stability of Ferrihydrite on Early Mars. *J. Geophys. Res. Planets* **122**, 358–382.

Dunlop D. J. and Ozdemir O. (1997) *Rock Magnetism: Fundamentals and frontiers*., Cambridge University Press, Cambridge.

Elkins-Tanton L. T., Weiss B. P. and Zuber M. T. (2011) Chondrites as samples of differentiated planetesimals. *Earth and Planetary Science Letters* **305**, 1–10.

Földvári M. (2011) *Handbook of thermogravimetric system of minerals and its use in geological practice*., Geological Inst. of Hungary, Budapest.

Ganino C. and Libourel G. (2017) Reduced and unstratified crust in CV chondrite parent body. *Nature Communications* **8**. Available at: http://www.nature.com/articles/s41467-017-00293-1 [Accessed January 9, 2019].

Garenne A., Beck P., Montes-Hernandez G., Chiriac R., Toche F., Quirico E., Bonal L. and Schmitt B. (2014) The abundance and stability of "water" in type 1 and 2 carbonaceous chondrites (CI, CM and CR). *Geochimica et Cosmochimica Acta* **137**, 93–112.

Gattacceca J., Suavet C., Rochette P., Weiss B. P., Winklhofer M., Uehara M. and Friedrich J. M. (2014) Metal phases in ordinary chondrites: Magnetic hysteresis properties and implications for thermal history. *Meteoritics & Planetary Science* **49**, 652–676.

Greenwood R. C., Franchi I. A., Kearsley A. T. and Alard O. (2010) The relationship between CK and CV chondrites. *Geochimica et Cosmochimica Acta* **74**, 1684–1705.

Grimm R. E. and McSween H. Y. (1989) Water and the thermal evolution of carbonaceous chondrite parent bodies. *Icarus* **82**, 244–280.

Guimon R. K., Symes S. J. K., Sears D. W. G. and Benoit P. H. (1995) Chemical and physical studies of type 3 chondrites XII: the metamorphic history of CV chondrites and their components. *Meteoritics* **30**, 704–714.

Howard K. T., Benedix G. K., Bland P. A. and Cressey G. (2010) Modal mineralogy of CV3 chondrites by X-ray diffraction (PSD-XRD). *Geochimica et Cosmochimica Acta* **74**, 5084–5097.

Howarth R. J. (1998) Improved estimators of uncertainty in proportions, point-counting, and pass-fail test results. *American Journal of Science* **298**, 594–607.

Huss G. R. and Lewis R. S. (1994) Noble gases in presolar diamonds II: component abundances reflect thermal processing. *Meteoritics* **29**, 811–829.

Huss G. R., Rubin A. E. and Grossman J. N. (2006) Thermal metamorphism in chondrites. In *Meteorites and the Early Solar System II* D.S. Lauretta and H.Y. McSween Jr., Tucson. pp. 567–586.

Ishida H., Nakamura T., Miura H. and Kakazu Y. (2012) Diverse mineralogical and oxygen isotopic signatures recorded in CV3 carbonaceous chondrites. *Polar Science* **6**, 252–

262.

Jarosewich E. (1990) Chemical analyses of meteorites - A compilation of stony and iron meteorite analyses. *Meteoritics* **25**, 323–337.

Jogo K., Nakamura T., Ito M., Wakita S., Zolotov M. Yu. and Messenger S. R. (2017) Mn–Cr ages and formation conditions of fayalite in CV3 carbonaceous chondrites: Constraints on the accretion ages of chondritic asteroids. *Geochimica et Cosmochimica Acta* **199**, 58–74.

Keller L. P. and Buseck P. R. (1990) Aqueous alteration in the Kaba CV3 carbonaceous chondrite. *Geochimica et Cosmochimica Acta* **54**, 2113–2120.

Keller L. P. and McKay D. S. (1993) Aqueous alteration of the Grosnaja CV3 carbonaceous chondrite. *Meteoritics* **28**, 378.

Keller L. P., Thomas K. L., Clayton R. N., Mayeda T. K., DeHart J. M. and McKay D. S. (1994) Aqueous alteration of the Bali CV3 chondrite: Evidence from mineralogy, mineral chemistry, and oxygen isotopic compositions. *Geochimica et Cosmochimica Acta* **58**, 5589–5598.

Kimura M. and Ikeda Y. (1998) Hydrous and anhydrous alterations of chondrules in Kaba and Mokoia CV chondrites. *Meteoritics & Planetary Science* **33**, 1139–1146.

King A. J., Solomon J. R., Schofield P. F. and Russell S. S. (2015) Characterising the CI and CI-like carbonaceous chondrites using thermogravimetric analysis and infrared spectroscopy. *Earth, Planets and Space* **67**.

Koblitz J. (2005) MetBase - Meteorite data retrieval software, version 7.1. Koblitz J. 2005.MetBase—Meteorite data retrieval software,version 7.1. Bremen, Germany: Koblitz. CD-ROM.

Krot A. N., Meibom A. and Keil K. (2000) A clast of Bali-like oxidized CV material in the reduced CV chondrite breccia Vigarano. *Meteoritics & Planetary Science* **35**, 817–825.

Krot A. N., Petaev M. I. and Bland P. A. (2004) Multiple formation mechanisms of ferrous olivine in CV carbonaceous chondrites during fluid-assisted metamorphism. *Antarct. Meteorite Res.* **17**, 153–171.

Krot A. N., Petaev M. I., Scott E. R. D., Choi B.-G., Zolensky M. E. and Keil K. (1998a) Progressive alteration in CV3 chondrites: More evidence for asteroidal alteration. *Meteoritics & Planetary Science* **33**, 1065–1085.

Krot A. N., Petaev M. I., Zolensky M. E., Keil K., Scott E. R. D. and Nakamura K. (1998b) Secondary calcium-iron-rich minerals in the Bali-like and Allende-like oxidized CV3 chondrites and Allende dark inclusions. *Meteoritics & Planetary Science* **33**, 623–645.

Krot A. N., Scott E. R. D. and Zolensky M. E. (1995) Mineralogical and chemical modification of components in CV3 chondrites: Nebular or asteroidal processing? *Meteoritics* **30**, 748–775.

Lee M. R., Hutchison R. and Graham A. L. (1996) Aqueous alteration in the matrix of the Vigarano (CV3) carbonaceous chondrite. *Meteoritics & Planetary Science* **31**, 477–483.

Lee T., Papanastassiou D. A. and Wasserburg G. J. (1977) Aluminum-26 in the early solar system - Fossil or fuel. *The Astrophysical Journal* **211**, L107.

Lunning N. G., Corrigan C. M., McSween H. Y., Tenner T. J., Kita N. T. and Bodnar R. J. (2016) CV and CM chondrite impact melts. *Geochimica et Cosmochimica Acta* **189**, 338–358.

MacPherson G. J. and Krot A. N. (2014) The formation of Ca-, Fe-rich silicates in reduced and oxidized CV chondrites: The roles of impact-modified porosity and permeability, and heterogeneous distribution of water ices. *Meteoritics & Planetary Science* **49**, 1250–1270.

Marrocchi Y., Bekaert D. V. and Piani L. (2018) Origin and abundance of water in carbonaceous asteroids. *Earth and Planetary Science Letters* **482**, 23–32.

McKeegan K. D. and Davis A. M. (2005) Early Solar System chronology. In *Meteorites, Comets and Planets: Treatise on Geochemistry* Elsevier B.V., Amsterdam, The Netherlands.

McSween H. Y. (1977) Petrographic variations among carbonaceous chondrites of the Vigarano type. *Geochimica et Cosmochimica Acta* **41**, 1777–1790.

McSween H. Y. J., Ghosh A., Grimm R. E., Wilson L. and Young E. D. (2002) Thermal evolution of models of asteroids. In *Asteroids III* University of Arizona Press.

Munayco P., Munayco J., de Avillez R. R., Valenzuela M., Rochette P., Gattacceca J. and Scorzelli R. B. (2013) Weathering of ordinary chondrites from the Atacama Desert, Chile, by Mössbauer spectroscopy and synchrotron radiation X-ray diffraction. *Meteoritics & Planetary Science* **48**, 457–473.

Nakato A., Nakamura T., Kitajima F. and Noguchi T. (2008) Evaluation of dehydration mechanism during heating of hydrous asteroids based on mineralogical and chemical analysis of naturally and experimentally heated CM chondrites. *Earth, Planets and Space* **60**, 855–864.

Nozaki W., Nakamura T. and Noguchi T. (2006) Bulk mineralogical changes of hydrous micrometeorites during heating in the upper atmosphere at temperatures below 1000 °C. *Meteoritics & Planetary Science* **41**, 1095–1114.

Raynal P. I., Quirico E., Borg J., Deboffle D., Dumas P., d 'Hendecourt L., Bibring J.-P. and Langevin Y. (2000) Synchrotron infrared microscopy of micron-sized extraterrestrial grains. *Planetary and Space Science* **48**, 1329–1339.

Rietmeijer F. J. M. and Mackinnon I. D. R. (1985) Poorly graphitized carbon as a new cosmothermometer for primitive extraterrestrial materials. *Nature* **315**, 733–736.

Rochette P., Gattacceca J., Bonal L., Bourot-Denise M., Chevrier V., Clerc J.-P., Consolmagno G., Folco L., Gounelle M., Kohout T., Pesonen L., Quirico E., Sagnotti L. and Skripnik A. (2008) Magnetic classification of stony meteorites: 2. Non-ordinary chondrites. *Meteoritics & Planetary Science* **43**, 959–980.

Rochette P., Sagnotti L., Bourot-Denise M., Consolmagno G., Folco L., Gattacceca J., Osete M. L. and Pesonen L. (2003) Magnetic classification of stony meteorites: 1. Ordinary chondrites. *Meteoritics & Planetary Science* **38**, 251–268.

Rubin A. E. (2012) Collisional facilitation of aqueous alteration of CM and CV carbonaceous chondrites. *Geochimica et Cosmochimica Acta* **90**, 181–194.

Rubin A. E. (1991) Euhedral awaruite in the Allende meteorite: implications for the origin of awaruite- and magnetite-bearing nodules in CV3 chondrites. **76**, 1356–1362.

Scott E. R. D., Keil K. and Stöffler D. (1992) Shock metamorphism of carbonaceous chondrites. *Geochimica et Cosmochimica Acta* **56**, 4281–4293.

Simon S. B., Grossman L., Casanova I., Symes S., Benoit P., Sears D. W. G. and Wacker J. F. (1995) Axtell, a new CV3 chondrite find from Texas. *Meteoritics* **30**, 42–46.

Sleep N. H., Meibom A., Fridriksson Th., Coleman R. G. and Bird D. K. (2004) H2-rich fluids from serpentinization: Geochemical and biotic implications. *Proceedings of the National Academy of Sciences* **101**, 12818–12823.

Tomeoka K. and Buseck P. R. (1990) Phyllosilicates in the Mokoia CV carbonaceous chondrite: Evidence for aqueous alteration in an oxidizing environment. *Geochimica et Cosmochimica Acta* **54**, 1745–1754.

Tomeoka K. and Tanimura I. (2000) Phyllosilicate-rich chondrule rims in the Vigarano CV3 chondrite: evidence for parent-body processes. *Geochimica et Cosmochimica Acta* **64**, 1971–1988.

Uehara M., Gattacceca J., Rochette P., Demory F. and Valenzuela E. M. (2012) Magnetic

study of meteorites recovered in the Atacama desert (Chile): Implications for meteorite paleomagnetism and the stability of hot desert surfaces. *Physics of the Earth and Planetary Interiors* **200–201**, 113–123.

Wasson J. T., Isa J. and Rubin A. E. (2013) Compositional and petrographic similarities of CV and CK chondrites: A single group with variations in textures and volatile concentrations attributable to impact heating, crushing and oxidation. *Geochimica et Cosmochimica Acta* **108**, 45–62.

Weinbruch S., Palme H., Muller W. F. and El Gorsey A. (1990) FeO-rich rims and veins in Allende forsterite - Evidence for high temperature condensation at oxidizing conditions. *Meteoritics* **25**, 115–125.

Weisberg M. K., Prinz M., Clayton R. N. and Mayeda T. K. (1997) CV3 chondrites: three subgroups, not two. *Meteoritics & Planetary Science* **32**, 138.

Yang C.-W., Williams D. B. and Goldstein J. I. (1997) Low-temperature phase decomposition in metal from iron, stony-iron, and stony meteorites. *Geochimica et Cosmochimica Acta* **61**, 2943–2956.

Journal Pre-proofs

sample	**Section/ sample number**	**source**	**Fall vs. find**	**shock stage**	**total area (cm²)**	**matrix (vol. %)**	**matrix /high-Temp. Components**
ALH 81003	14	MWG	f	S2	0.32	53.7	1.16
ALH 84028	11	MWG	f	S1	1.72	51.5	1.06
ALH 85006	47	MWG	f	S3	1.19	48.2	0.93
Allende	3181-2, -2b, -3	MNHN	Fall	S1*	6.27	50.2	1.01
Axtell	ME3203.5	FMNH	f	-	1.95	44.1	0.79
Bali	4839	CEREGE MNHN	Fall	S3*	3.35	49.9	1.00
Bukhara	N16697	Verdnasky	Fall	S1	1.45	39.3 ▲	0.65
Efremovka	3125-1	MNHN	f	S4*	1.18	19.4	0.24
GRA 06101	37	MWG	f	---			
GRA 06130	7	MWG	f	S2	0.49	49.5	0.81
GRO 95652	10	MWG	f	S2	0.75	37.1	0.59
Grosnaja	ME1732.13, ME1732.19	FMNH	Fall	S3*	1.52	69.6	2.29
Kaba	88-1	MNHN	Fall	S1*	0.56	52.7	1.11
LAP 02206	36	MWG	f	S1	0.72	44.8	0.81
LAR 06317	23	MWG	f	S3	1.00	60.2	1.51
LAR 06867	7	MWG	f	S3	0.70	52.9	1.12
Leoville	1, 3209	MNHN	f	S3	2.42	31.7	0.46
MCY 05219	14	MWG	f	S3	0.73	54.1	1.18
MET 00430	6	MWG	f	S2	1.09	48.0	0.92
MET 00671	4	MWG	f	S2	0.55	39.8	0.66
MET 01074	11	MWG	f	S2	0.65	39.8	0.66
MIL 07002	11	MWG	f	S2	1.00	41.9	0.72
MIL 07277	7	MWG	f	S3	0.90	45.2	0.82
MIL 07671	13	MWG	f	S3	0.74	45.5	0.84
MIL 091010	20	MWG	f	S2	1.21	46.4	0.87
Mokoia	P10420, P13282	NHM	Fall	S1*	0.34	42.6	0.74
QUE 94688	7	MWG	f	S2	0.76	62.1	1.64
QUE 97186	11	MWG	f	S2	0.90	44.1 ▲	0.79
RBT 04143	11	MWG	f	S3	1.47	34.1	0.52
RBT 04302	7	MWG	f	S2	0.92	38.2	0.62
Vigarano	2793-1, 2	MNHN	Fall	S1-S2*	2.85	35.1	0.54

Journal Pre-proofs

Table 1: **Sample list, Fall or find, with the specific considered section number and sources, shock level, and matrix abundances.**

ALH stands for Allan Hills, GRA for Graves Nunataks, GRO for Grosvenor Mountains, LAP for LaPaz Icefield, LAR for Larkman Nunatak, MCY for MacKay Glacier, MET for Meteorite Hills, MIL for Miller Range, QUE for Queen Alexandra Range, and RBT for Roberts Massif. Shock levels were either established in the present work or previously (as specified with the * symbol) by McSween (1977) and Scott et al. (1992). According to our observations, RBT 04143 experienced significant shock (S3), in agreement with Lunning et al. (2016). Matrix abundances were all evaluated though image analysis, at the exception of QUE 97186 and Bukhara, for which point counting was used (▲).

FMNH: Field Museum of Natural History (Chicago – USA) MWG: Meteorite Working Group at NASA Johnson Space Center (Houston – USA); MNHN: Museum National d'Histoire Naturelle (Paris – France); CEREGE (Aix-en-Provence – France); Vernadsky Institute of Geochemistry and Analytical Chemistry of Russian Academy of Sciences (Moscow, Russia). It should be noted that the section "37" of GRA 06101, that was loaned to us consists of a single large igneous inclusion. It does not exhibit matrix and chondrules, preventing the determination of matrix abundance.

Journal Pre-proofs

	metal						sulfides			magnetic properties		
	modal abundance			average Ni content								
CV	**average (vol. %)**	**95% interval confidence (vol. %)**	**n points**	**Ni (wt%)**	**sd**	**n**	**average Ni content (wt. %)**	**sd**	**n**	**Magnetic susceptibility logχ (χ in 10^{-9} m^3kg^{-1})**	**Saturation magnetization M_S (Am^2kg^{-1})**	**Saturation remanence M_{RS} (Am^2kg^{-1})**
ALH 81003	0.15	[0.01 – 0.82]	676	67.2	4.8	10	13.2	7.5	20	3.68 ✧	0.66	0.069
ALH 84028	1.01	[0.52 – 1.76]	1192	66.3	1.1	4	8.1	10.7	20	3.92 ✧	1.17	0.055
ALH 85006	0.09	[0.00 – 0.50]	1113	-	-	-	28.4	1.8	10	4.52 ✧	5.52	1.23
Allende	0.20*	[0.04 – 0.57]	1572	57.1*	23	26	11.4*	11.5	21	3.62 ✧	0.61	0.063
Axtell	0.00	[0.00 – 1.11]	630	67.5	1.4	2	11.7	9.8	7	3.14 ✧	0.09	0.017
Bali	0.00 *	[0.00 – 0.33]	2103	16.0*	14	2	16.6*	5.9	20	4.27 ✧	3.43	0.94
Bukhara	2.23	[1.28 – 3.60]	716	27.7	20.3	25	0.1	0.2	10	4.37 ✧	10.2	0.38
Efremovka	4.60*	[3.63 – 5.74]	1611	1.6*	2.5	30	0.0*	0	15	4.83 ✧	18.7	0.65
GRA 06101	no section available									3.82	1.05	0.058
GRA 06130	0.73	[0.27 – 1.59]	818	67.9	0.2	10	7.1	8.7	20	3.77	0.83	0.049
GRO 95652	3.12	[2.13 – 4.4]	995	27.1	19.6	10	0.1	0.1	10	4.23 ✧	4.39	0.24
Grosnaja	tr*	[0.00 – 0.37]	1885	-	-	-	17.5*	8.2	15	3.97 ✧	1.99	0.60
Kaba	0.00*	[0.00 – 0.45]	1561	3.7*	1.2	6	10.6*	8.5	19	4.85 ✧	10.4	1.69
LAP 02206	1.15	[0.68 – 1.81]	1563	69.7	0.2	10	8.0	9.8	45	3.69 ✧	0.40	0.03
LAR 06317	0.17	[0.00 – 0.73]	1000	-	-	-	20.9	15.7	20	4.37	3.88	0.82
LAR 06867	0.19	[0.02 – 0.66]	1102	-	-	-	17.3	10.1	20	3.95	2.39	0.68
Leoville	1.80*	[1.21 – 2.53]	1718	10.1*	12.9	30	0.4*	1.1	15	4.53 ✧	5.86	0.63
MCY 05219	0.00	[0.00 – 0.99]	704	-	-	-	13.6	10	20	4.33	3.85	1.01
MET 00430	0.00	[0.00 – 0.77]	906				15.1	7.6	20	4.63 ✧	10.3	2.53
MET 00761				-	-	-				4.63 ✧	10.1	2.27

Journal Preproofs

MET 01074										4.63 ✧	9.48	2.49
MIL 07002	0.54	[0.25 – 1.02]	1664	66.5		1	3.9	6.1	20	3.79	1.12	0.66
MIL 07277	4.10	[2.70 – 5.95]	634	20.7	18.2	24	0.1	0.2	30	4.65	11.3	0.55
MIL 07671	0.80	[0.37 – 1.51]	1124	66.5	0.1	2	5.8	7.1	20	3.84	1.14	0.060
MIL 091010	0.28	[0.06 – 0.81]	1084	67.8	0.1	2	3.9	6.7	20	3.48	0.46	0.078
Mokoia	0.00*	[0.00 – 0.46]	1510	-	-	-	13.6*	6.6	18	4.6 ✧	7.16	1.31
QUE 94688	0.09	[0.01 – 0.49]	1143	-	-	-	3.8	5.4	22	3.07 ✧	0.16	0.030
QUE 97186	3.05	[1.92 – 4.58]	721	26.3	18.9	15	0.2	0.3	10	4.01 ✧	3.09	0.43
RBT 04143	1.66	[0.99 – 2.61]	1087	29.3	19	28	2.6	7.1	43	4.48	9.50	0.89
RBT 04302	2.07	[1.25 – 3.21]	920	27.1	16.3	15	0.0	0.0	10	4.45	6.97	0.93
Vigarano	1.29*	[0.84 – 1.97]	2631	21.1*	18.3	27	0.5*	2.9	15	4.36 ✧	6.21	0.98

Table 2: Opaque minerals in the studied CV chondrites.

Modal abundances of metal (average and 95% confidence intervals), average Ni contents (in wt. %) of metal and sulfides, and magnetic properties of CV chondrites. “n” represents the number of counts for the modal abundances and the number of analyses for the average Ni contents of metal and sulfides. “sd” stands for the standard deviations, and “tr” for trace. We did not observe metal in the section of Grosnaja. Unless specified by “*” (McSween, 1977) and by “✧” (Rochette et al. 2008), data are all from the present study. Vigarano is the only chondrite were data from both the present work and McSween (1977) were compiled.

Journal Pre-proofs

	total mass loss (wt. %)				total mass loss (wt. %) Mat. Norm.
CV	**[0-200°C]**	**[200-350°C]**	**[350-850 °C]**	**[200 -900°C]**	**[200 -900°C]**
ALH 81003	0.25	0.11	0.06	0.23	0.43
ALH 84028	0.25	0.23	0.16	0.44	0.85
ALH 85006	1.42	0.71	2.48	3.26	6.75
Allende	0.56	0.29	0.33	0.77	1.53
Axtell (†)	1.23	1.12	1.28	2.44	5.54
Bali	0.94	0.36	1.21	2.01	4.03
Bukhara	0.91	0.87	0.17	1.04	2.65
Efremovka	-	-	-	-	-
GRA 06101	0.27	0.23	0.21	0.54	-
GRA 06130	0.46	0.21	0.30	0.55	1.11
GRO 95652 (†)	1.33	1.27	1.99	3.66	9.88
Grosnaja	1.00	0.64	2.01	2.90	4.17
Kaba	1.46	0.71	3.34	4.48	8.5
LAP 02206	0.39	0.22	0.22	0.50	1.12
LAR 06317	1.98	0.54	2.87	3.43	5.7
LAR 06867 (†)	3.48	1.43	3.19	4.75	8.97
Leoville	1.03	1.03	1.57	2.97	9.38
MCY 05219	0.38	0.22	1.13	1.48	2.74
MET 00430	0.55	0.20	1.31	1.6	3.34
MET 00761	1.04	0.61	1.31	2.18	5.49
MET 01074	0.40	0.24	1.28	1.64	4.13
MIL 07002	0.57	0.28	0.51	0.89	2.12
MIL 07277	1.00	0.52	0.74	1.48	3.28
MIL 07671	0.54	0.34	0.47	0.86	1.89
MIL 091010 (†)	1.66	0.96	2.26	3.32	7.17
Mokoia	0.46	0.27	1.07	1.82	4.26
QUE 94688 (†)	3.17	1.25	2.89	4.33	6.97
QUE 97186	1.01	0.70	1.30	2.05	3.66
RBT 04143	1.58	0.84	1.10	1.92	5.64
RBT 04302	1.63	1.00	1.55	2.76	7.22
Vigarano	0.95	0.98	1.96	3.13	8.91

Table 3: Summary of mass losses in the studied CV chondrites as a function of temperature by TGA. Some samples **(†)** are identified as terrestrially weathered: they are particularly enriched in water released at T < 200°C (QUE 94688, LAR 06867) or in oxy-hydroxides (GRO 95652, LAR 06867, QUE 94688, Axtell, MIL 091010).

Journal Pre-proofs

sample	preparation	n	$FWHM_D$ (cm^{-1})	I_D/I_G	PT
ALH 85006	bulk	30	121.3 +/- 33.0	0.96 +/- 0.20	3.6
	section	36	116.4 +/- 16.4	0.96 +/- 0.07	3.6
LAR 06867	section	38	83.8 +/- 7.3	1.35 +/- 0.07	3.6
ALH 84028	section	38	72.2 +/- 11.3	1.49 +/- 0.11	3.7
GRA 06130	section	39	69.0 +/- 9.4	1.51 +/- 0.11	3.7
MIL 07002	section	39	68.8 +/- 9.2	1.57 +/- 0.08	3.7
MIL 07671*	section	25	68.8 +/- 7.6	1.52 +/- 0.08	3.7
Bukhara	bulk	32	94.3 +/- 7.23	1,29 +/- 0.06	>3.6

Table 4: **CV chondrites and their respective Raman spectral parameters**. The spectral parameters ($FWHM_D$, I_D/I_G) were obtained through the reduction of n spectra and interpreted to attribute a petrologic type (PT).

Journal Pre-proofs

pairing	meteorites	Classif.	logχ (χ in 10^{-9} m^3kg^{-1})	M_{RS}/M_S	Raman		total mass loss (wt. %)
					$FWHM_D$ (cm^{-1})	I_D/I_G	
most likely paired	**MET 00430**	Ox_B	4.69	0.24	113.2+/- 4.8	1.00 +/- 0.03	1.17
	MET 00671	Ox_B	4.69	0.21	117.9 +/- 4.9	0.98 +/- 0.01	1.79
	MET 01074	Ox_B	4.69	0.26	112.5 +/- 4.9	0.98 +/- 0.02	1.64
most likely paired	**MIL 07002**	Ox_A	3.79	0.06	68.8 +/- 9.2	1.57 +/- 0.08	0.85
	MIL 07671	Ox_A	3.84	0.05	68.8 +/- 7.62	1.52 +/- 0.08	0.82
Unpaired	**MIL 091010**	Ox_A	3.48	0.17	75.5 +/- 5.8	1.49 +/- 0.06	3.26
	MIL 07277	Red	4.65	0.05	131.3+/- 24.7	1.08 +/- 0.09	1.48

Table 5: Pairing of Antarctic CV chondrites. The total mass losses (in wt. %) are measured by TGA.

Journal Pre-proofs

	Meteorites	matrix (vol. %)	Ni (wt. %) in sulfides	metal abundance (vol. %)	Ni (wt. %) in metal	saturation remanence M_{RS} (Am^2kg^{-1})	Magnetic susceptibility logχ (χ in 10^{-9} m^3kg^{-1})	Saturation magnetization M_S (Am^2kg^{-1})
OxA	**ALH 81003**	53.7	13.2	0.15	67.2	0.069	3.68	0.66
	ALH 84028	51.5	8.1	1.01	66.3	0.055	3.92	1.17
	Allende	50.2	11.4	0.2	57.1	0.063	3.62	0.61
	Axtell	44.1	11.7	*tr*	67.5	0.017	3.14	0.09
	GRA 06101					0.058	3.82	1.05
	GRA 06130	49.5	7.1	0.73	67.9	0.049	3.77	0.83
	LAP 02206	44.8	8.0	1.15	69.7	0.035	3.69	0.40
	MIL 07002	41.9	3.9	0.54	66.5	0.066	3.79	1.02
	MIL 07671	45.5	5.8	0.8	66.5	0.060	3.84	1.14
	MIL 091010	46.4	3.9	0.28	67.8	0.078	3.48	0.46
	QUE 94688	62.1	3.8	0.15		0.030	3.07	0.17
OxB	**ALH 85006**	48.2	28.4	0.16		1.23	4.52	5.52
	Bali	49.9	16.6	0.0	16	0.94	4.27	3.43
	Grosnaja	69.6	17.5	none		0.60	3.97	1.99
	Kaba	52.7	10.6	0	3.7	1.69	4.85	10.4
	LAR 06317	60.2	20.9	0.17		0.82	4.37	3.88
	LAR 06867	52.9	17.3	0.19		0.68	3.95	2.39
	MCY 05219	54.1	13.6	0.0		1.01	4.33	3.85
	MET 00430	48.0	15.1	0.0		2.53	4.63	10.3
	MET 00761	39.8				2.27	4.63	
	MET 01074	39.8				2.49	4.63	
	Mokoia	42.6	13.6	0.0		1.31	4.6	7.16
Red	**Bukhara**	39.3	0.05	2.23	27.7	0.38	4.37	10.2
	Efremovka	19.4	0.00	4.60	1.6	0.65	4.83	18.7
	GRO 95652	37.1	0.05	3.77	27.1	0.25	4.23	4.39
	Leoville	31.7	0.40	1.80	10.1	0.63	4.53	5.86

Journal Pre-proofs

MIL 07277	45.2	0.1	4.1	20.7	0.55	4.65	11.3
QUE 97186	44.1	0.2	3.05	26.3	0.44	4.01	3.09
RBT 04143	34.1	2.6	1.66	29.3	0.89	4.48	9.50
RBT 04302	38.2	0	2.07	27.1	0.93	4.45	6.97
Vigarano	35.1	0.5	1.29	21.1	0.98	4.36	6.21
average (OxA)	48.9 ± 5.6	7.5 ± 3.3	0.5 ± 0.38	66.28 ± 3.39	0.05 ± 0.02	3.62 ± 0.27	0.69 ± 0.37
average (OxB)	52.3 ± 8.5	16.4 ± 4.9	0.06 ± 0.08	9.85 ± 6.15	1.20 ± 0.55	4.43 ± 0.27	5.44 ± 3.01
average (Ox)	50.4 ± 7.3	11.3 ± 6.2	0.29 ± 0.36	56.02 ± 22.13	0.60 ± 0.70	4.03 ± 0.49	2.83 ± 3.20
average (Red)	35.1 ± 7.2	0.8 ± 0.8	2.73 ± 1.12	21.2 ± 8.89	0.60 ± 0.25	4.43 ± 0.22	8.47 ± 4.43

Table 6: Sub-classification of the studied CV chondrites. Petrographic, mineralogical and magnetic properties for classification of CV chondrites into three subgroups (CV_{OxA}, CV_{OxB}, CV_{Red}). When only traces of metal were observed, *tr* is indicated. Grosnaja is the only chondrite where metal was not observed at all.

Journal Pre-proofs

	Abundance of Fe,Ni metal (vol. %)	**average Ni content in sulfides (wt. %)**	**average Ni content in metal (wt. %)**	**M_{RS} (Am^2kg^{-1})**	**M_S (Am^2kg^{-1})**	**logχ (χ in 10^{-9} m^3kg^{-1})**
CV_{OxA}	< 1.2	> 3	> 55	< 0.08	< 1.2	< 4.0
CV_{OxB}	< 0.2	> 10	< 20	> 0.60	> 2.0	> 3.9
CV_{Red}	> 1.0	< 3	< 30	> 0.20	> 3.0	> 4.0

Table 7: Quantitative relevant parameters for separation of CV_{OxA}, CV_{OxB} and CV_{Red}.

Note that the magnetic parameters can be affected by terrestrial weathering and must be used with caution for strongly weathered metal-bearing meteorites. M_S and χ will decrease with increasing weathering whereas M_{RS} will be affected in a more unpredictable manner (see Uehara et al. 2012). Strong weathering may also bias the average Ni content of Fe,Ni metal towards higher values because high Ni-metal is more resistant to weathering than kamacite.

Journal Pre-proofs

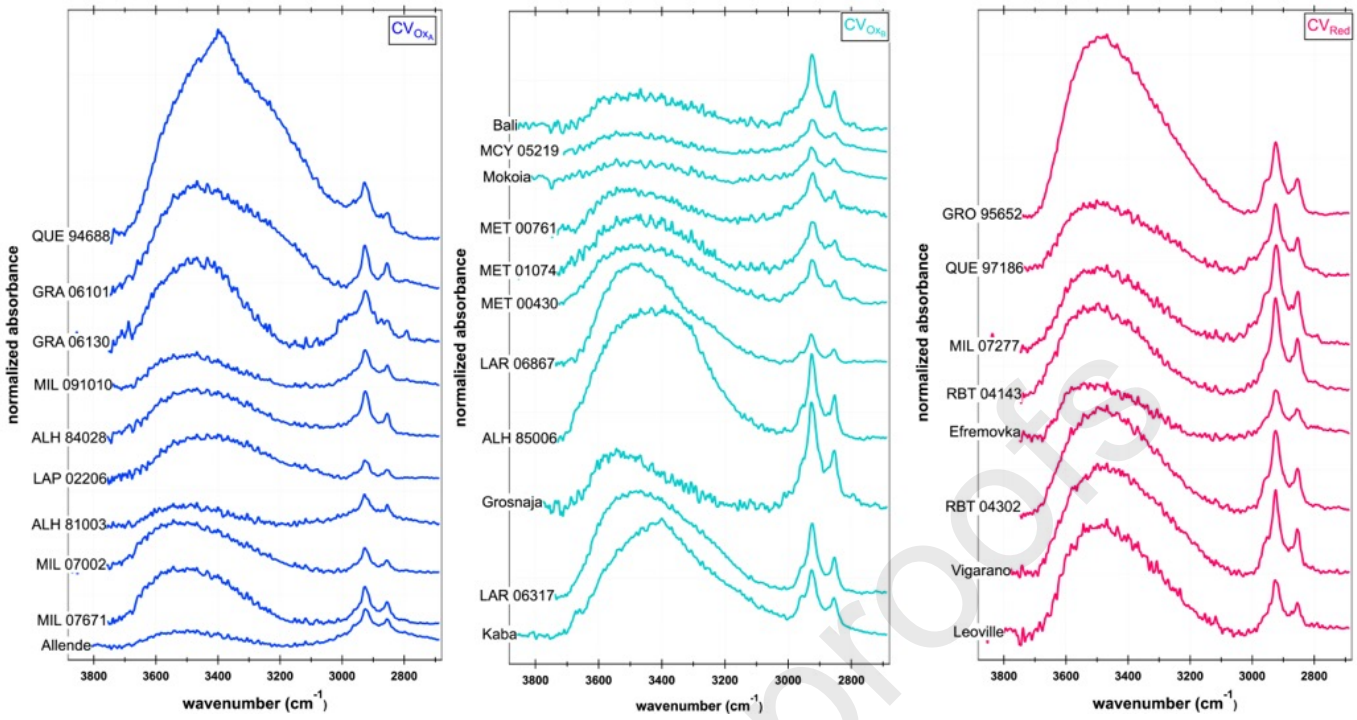

Fig. 1: Individual average IR spectra in transmission of matrix fragments of the considered series of CV chondrites, acquired at T = 100 °C. All spectra were baseline-corrected, normalized to the maximum of the Si-O band. Each chondrite exhibits the water band. A vertical offset was applied to ease the comparison of the spectra. CV_{OxA} appear in dark blue, CV_{OxB} in cyan and CV_{Red} in red (see text for explanation on the classification).

Journal Pre-proofs

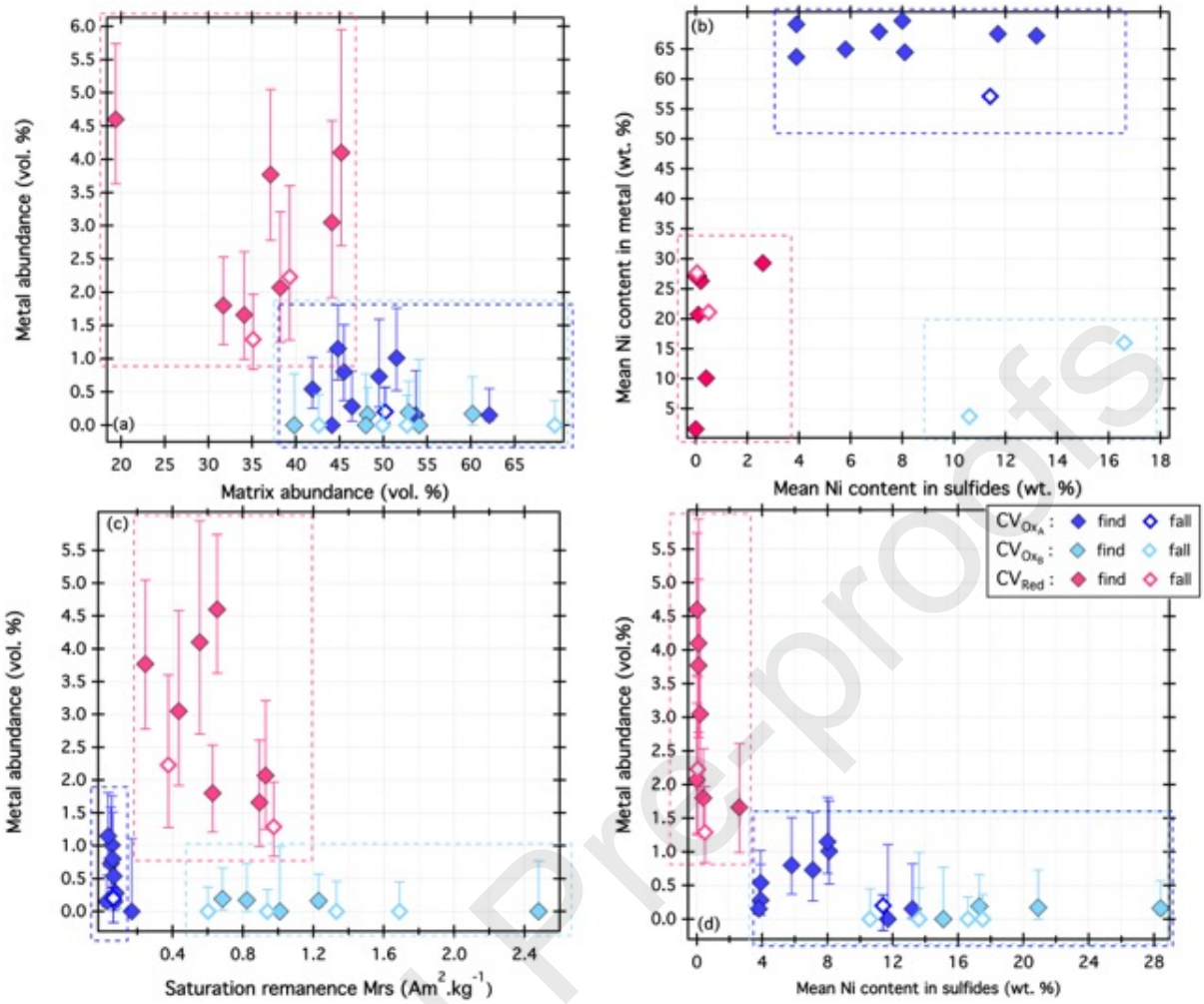

Fig. 2: Petrographic, mineralogical and magnetic properties of the three subgroups (CV_{OxA}, CV_{OxB}, CV_{Red}) (a) Metal abundance *vs.* matrix abundance ((b) mean Ni contents in sulfides *vs.* metal grains; (c) metal abundance *vs.* saturation remanence; (d) metal abundance *vs.* the mean Ni contents in sulfides for each CV chondrite considered in the present study. The 95 % interval confidence on the metal abundances are plotted for each chondrite. The dotted rectangles mark out the range of variability of the parameters for CV_{Red}, CV_{OxA} and CV_{OxB}.

Journal Pre-proofs

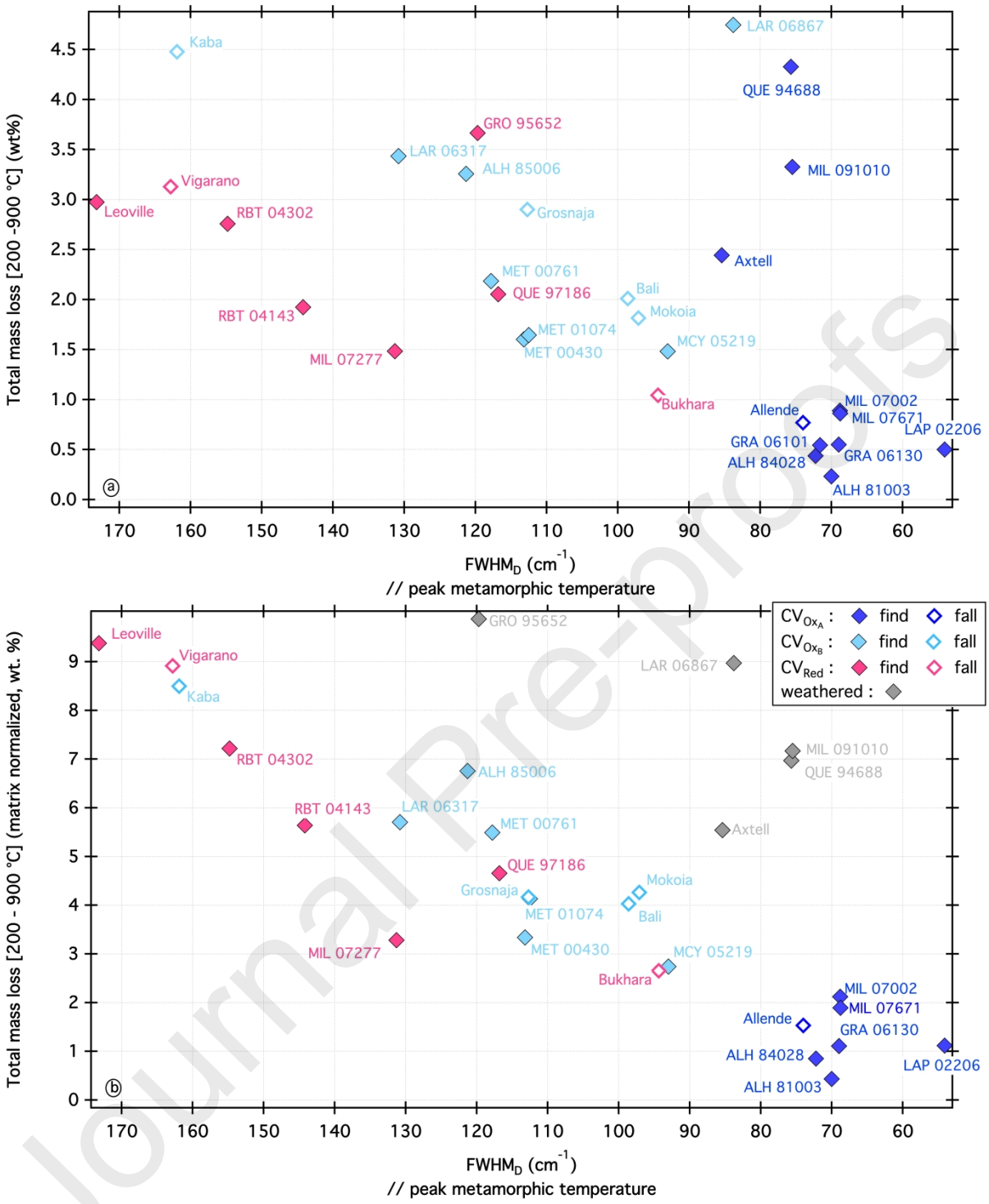

Fig. 3: Total mass loss (raw (a) and matrix-normalized (b) data) between 200 and 900 °C *vs.* the spectral Raman parameter $FWHM_D$. $FWHM_D$ is a proxy of the peak metamorphic temperature (see text).

Journal Pre-proofs

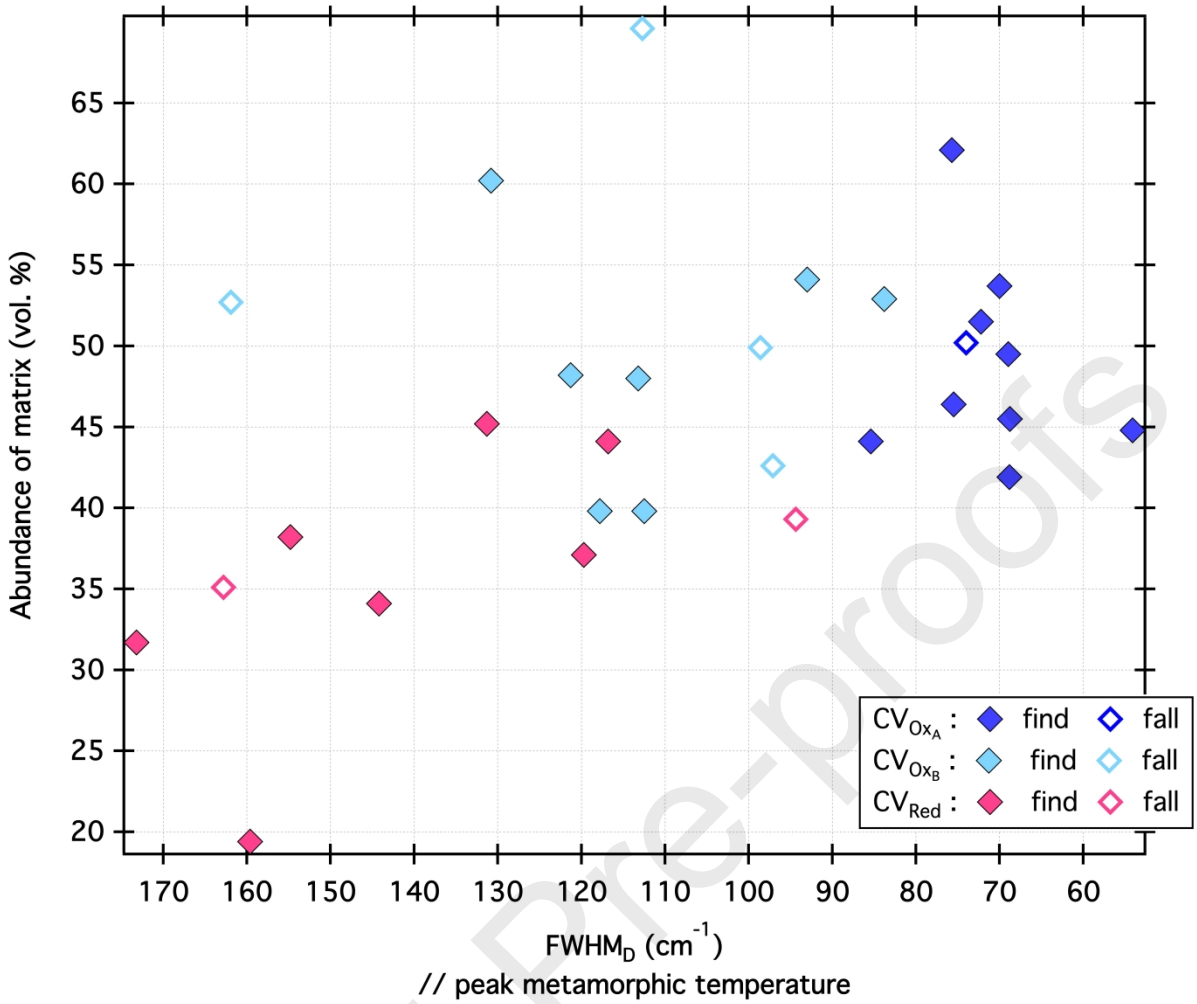

Fig. 4: Abundance of matrix as a function of the Raman spectral parameter $FWHM_D$ for individual CV chondrites.

Journal Pre-proofs

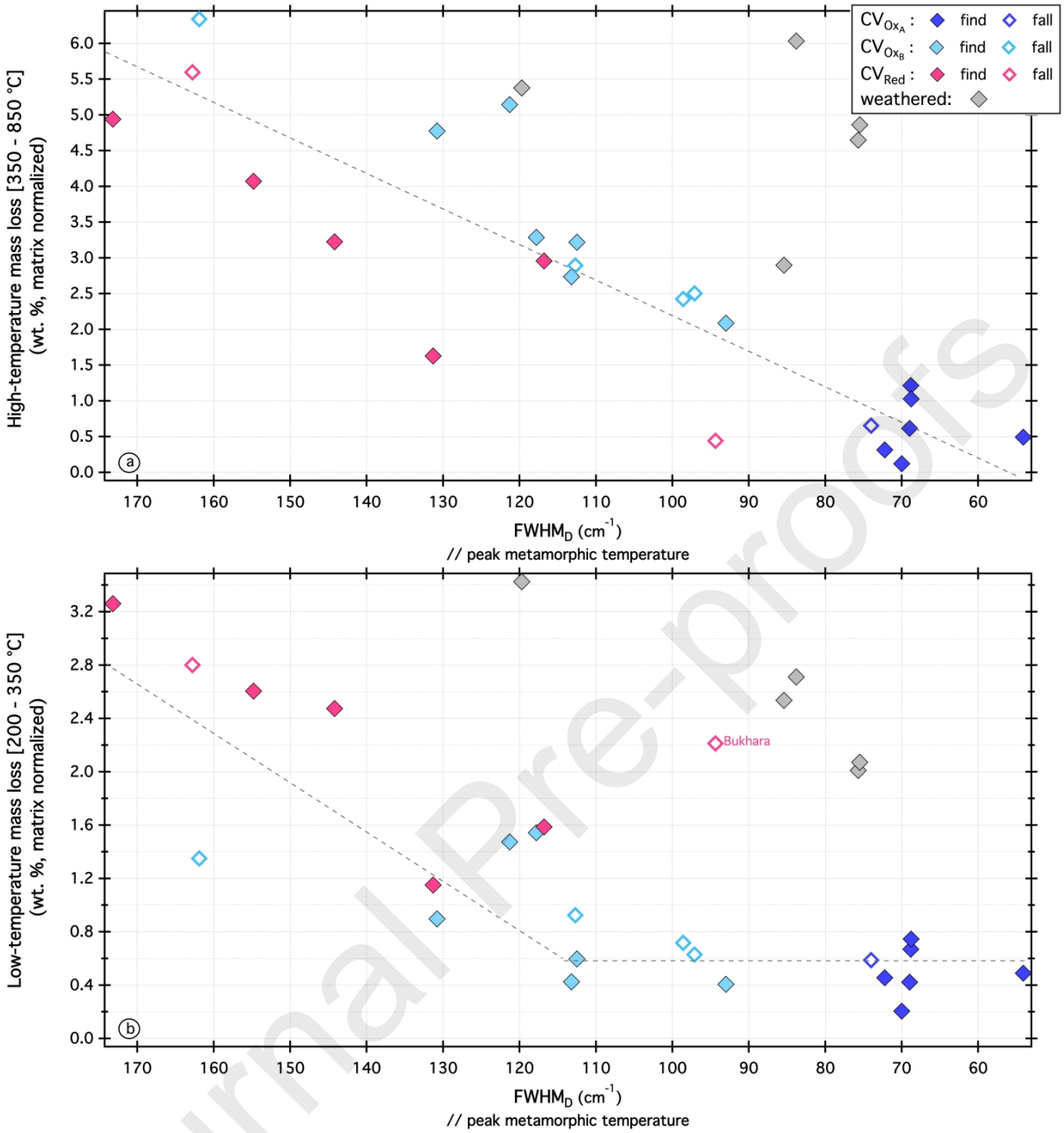

Fig. 5: Matrix-normalized high-temperature [350 - 850 °C] (a) and low-temperature [200 - 350 °C] (b) mass losses *vs.* the spectral Raman parameter $FWHM_D$. $FWHM_D$ is a proxy of the peak metamorphic temperature (see text).

Journal Pre-proofs

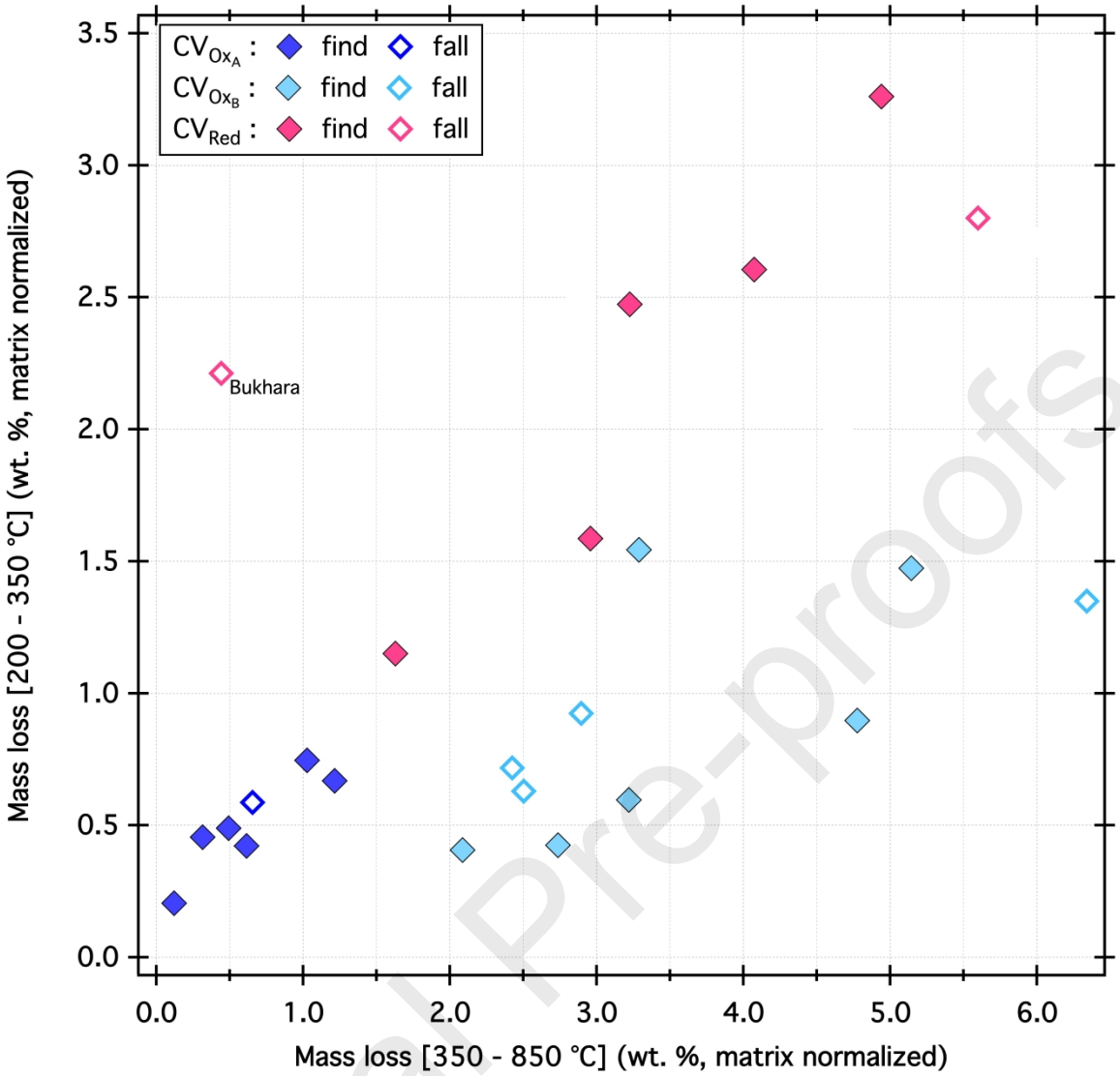

Fig. 6: Mass loss over the temperature range [200 - 350 °C] as a function of the mass loss over the temperature range [350 -850 °C] for CV_{OxA}, CV_{OxB}, and CV_{Red}. Data from weathered meteorites (QUE 94688, LAR 06867, Axtell, GRO 95652, and MIL 091010) are encircled. The low-temperature mass loss is mostly controlled by the decomposition of oxy-hydroxides, while the mass loss over the higher temperature range is mostly controlled by the de-hydroxylation of phyllosilicates (see text for details). CV_{Red} appear to be enriched in oxy-hydroxides in comparison to CV_{Ox}.

Journal Pre-proofs

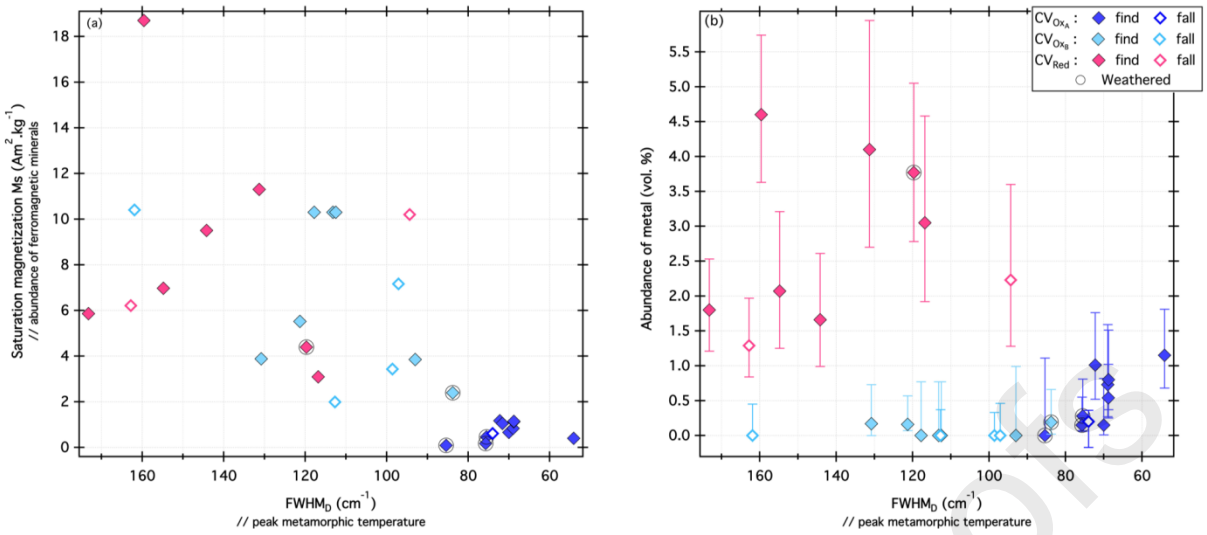

Fig. 7: (a) Saturation magnetization M_S and (b) abundance of metal as a function of the Raman parameter $FWHM_D$ for CV_{OxA}, CV_{OxB} and CV_{Red}. The 95 % interval confidence on the metal abundances are plotted for each chondrite.

Journal Pre-proofs

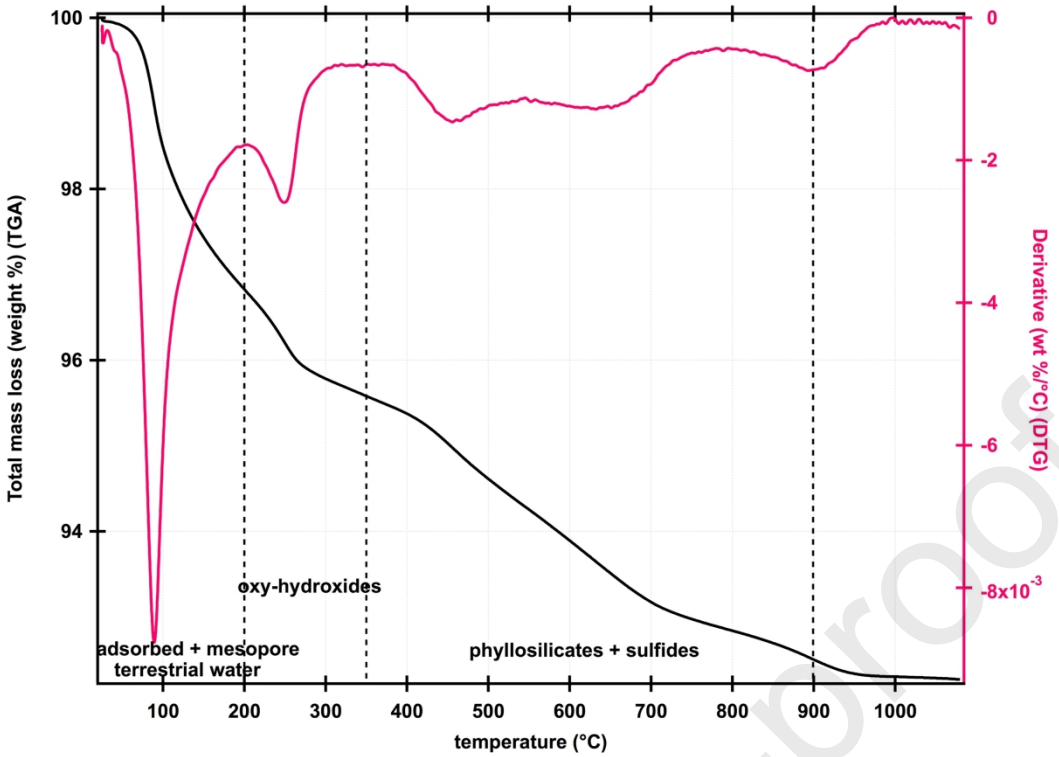

Fig. SOM1: TGA and DTG curves obtained on the bulk sample QUE 94688. Decomposition in different types of minerals as a function of temperature.

Journal Pre-proofs

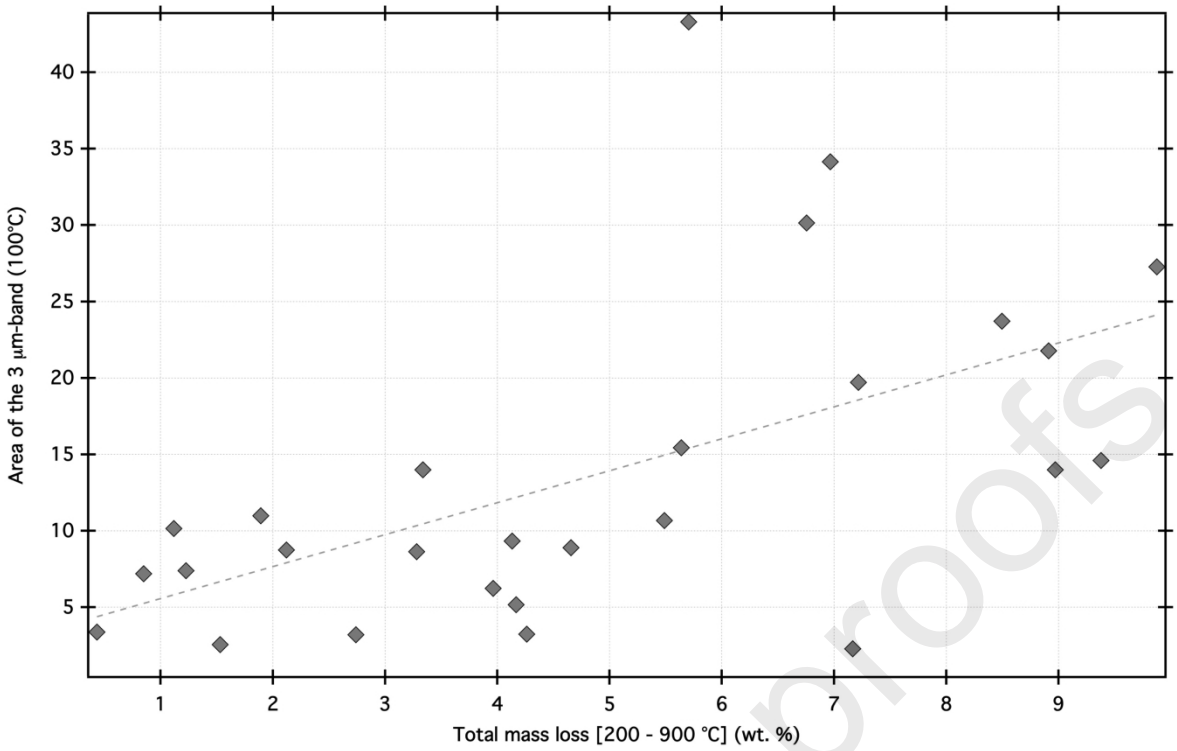

Fig. SOM2: Comparison of the parameters related to hydration retrieved from IR spectra and TGA measurements.

Journal Pre-proofs

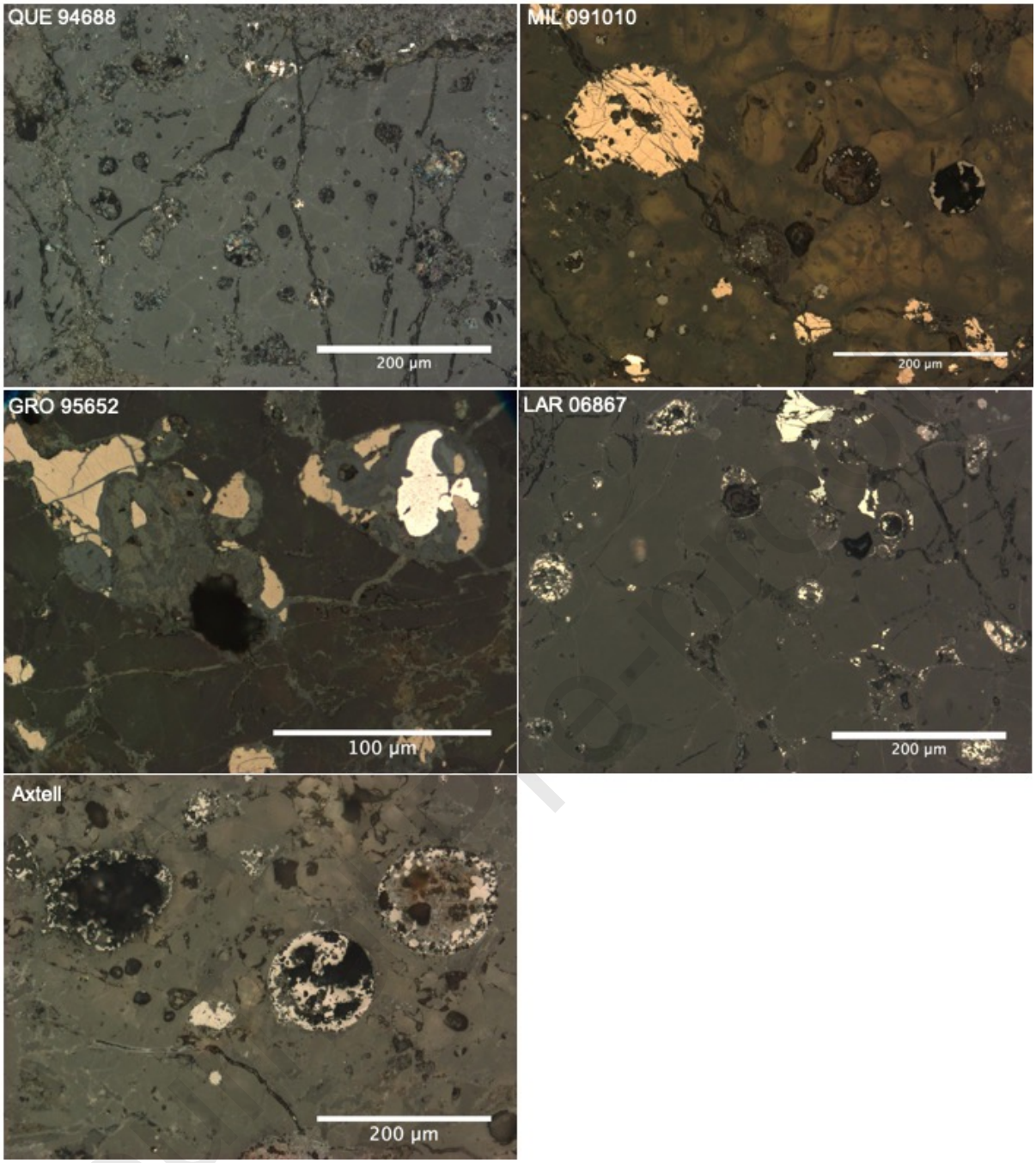

Fig. SOM3: Optical images of QUE 94688, MIL 091010, GRO 95652, LAR 06967, and Axtell in reflected light showing the presence of corroded metal grains. Veins filled by terrestrial weathering products are visible in GRO 95652 and Axtell.

Declaration of interests: none

☒ The authors declare that they have no known competing financial interests or personal relationships that could have appeared to influence the work reported in this paper.

☐The authors declare the following financial interests/personal relationships which may be considered as potential competing interests:

Journal Pre-proofs